



저작자표시-비영리-변경금지 2.0 대한민국

이용자는 아래의 조건을 따르는 경우에 한하여 자유롭게

- 이 저작물을 복제, 배포, 전송, 전시, 공연 및 방송할 수 있습니다.

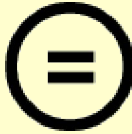
다음과 같은 조건을 따라야 합니다:



저작자표시. 귀하는 원저작자를 표시하여야 합니다.



비영리. 귀하는 이 저작물을 영리 목적으로 이용할 수 없습니다.



변경금지. 귀하는 이 저작물을 개작, 변형 또는 가공할 수 없습니다.

- 귀하는, 이 저작물의 재이용이나 배포의 경우, 이 저작물에 적용된 이용허락조건을 명확하게 나타내어야 합니다.
- 저작권자로부터 별도의 허가를 받으면 이러한 조건들은 적용되지 않습니다.

저작권법에 따른 이용자의 권리는 위의 내용에 의하여 영향을 받지 않습니다.

이것은 [이용허락규약\(Legal Code\)](#)을 이해하기 쉽게 요약한 것입니다.

[Disclaimer](#)

Master's Thesis

Compact and cross-linked nanoparticles: nano-
platform for highly stable, versatile conjugation and
its bio-application

Im Kyung Han

Department of Chemical Engineering

Graduate School of UNIST

2018

Compact and cross-linked nanoparticles: nano-
platform for highly stable, versatile conjugation
and its bio-application

Im Kyung Han

Department of Chemical Engineering

Graduate School of UNIST

Compact and cross-linked nanoparticles: nano-
platform for highly stable, versatile conjugation
and its bio-application

A thesis/dissertation
submitted to the Graduate School of UNIST
in partial fulfillment of the
requirements for the degree of
Master of Science

Im Kyung Han

12/11/2017 of submission

Approved by



Advisor

Jongnam Park

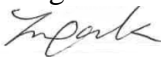
Compact and cross-linked nanoparticles: nano-
platform for highly stable, versatile conjugation
and its bio-application

Im Kyung Han

This certifies that the thesis/dissertation of Im Kyung Han is
approved.

12/11/2017 of submission

signature

_____  _____

Advisor: Jongnam Park

signature

_____  _____

Chang Young Lee: Thesis Committee Member #1

signature

_____  _____

Hyun-Woo Rhee: Thesis Committee Member #2

Abstract

Iron oxide nanoparticles (IONPs) have been investigated enormously in bio-application field including MRI contrast image, cancer cell targeting, biological sensing, and drug delivery. All these bio applicable IONPs require highly monodisperse size, biocompatibility, and long term colloidal stability in aqueous media.

The synthesis of high quality IONPs was reported in the previous study. However, these uniform sizes of IONPs are constructed with hydrophobic ligand because they are synthesized in oil phase. In addition, IONPs for bio application, the surface modification step is essential. There are two main surface modification methods, ligand exchange and encapsulation with amphiphilic polymers, have been employed to produce water dispersible and biocompatible IONPs. Although encapsulation process is easy, rapid, and reproducible, there are limitations of poor purification of polymer micelle structure and increase in hydrodynamic diameter size. In this research, to overcome these limitations, ligand exchange with random copolymer which was synthesized by RAFT polymerization was used to synthesize highly compact and robust water dispersible IONPs.

After 12 nm of IONPs were ligand exchanged with optimized ligand, these were maintained compact HD size about $\sim 15 \pm 4$ nm with high yield and reproducibility. Although their colloidal stability was established, functionalization of IONPs and stability in further reactions to conjugate bio molecules were required. To achieve these requirements, 'cross-linking' using various length of diamine was investigated in this research. Cross-linking reaction proceeded by EDC coupling of diamine and carboxyl group of IONPs surface ligand. From this process, highly enhanced colloidal stability of IONPs and functionalization of amine group were expected. To confirm the cross-linked nanoparticles (CLNPs), XPS spectra and visualization with TEM analysis were performed. CLNPs enhanced stability was compared with PEG dominant ligand (IONPs-PEG) and acid included ligand (IONPs-AA) composed IONPs by broad range of pHs, NaCl solution, temperature, purification effects and 'click chemistry' condition. These were evaluated by changes of each conditions of IONPs sizes with DLS analysis. Furthermore, as available functionalized amines of CLNPs were observed by RITC conjugation, tried to conjugate two different bio molecules. One is mannose carbohydrate conjugation was proceeded and confirmed with HR-MAS analysis and FT-IR. Also, MR relaxivity was measured by concanavalin A (Con A) mannose selective binding lectin to confirm conjugated mannose was retained their property. The other approach was folic acid conjugation. With folic acid conjugated CLNPs (CLNPs-FA), in vitro test was performed. HeLa cell which have lots of folate receptor on their surface was used to evaluate CLNPs-FA targeting ability. The result of targeting was observed with Prussian blue staining of HeLa cell.

Through this research, compact and robust ligand and cross-linking conditions were optimized and

confirmed various tool. At the same time, amine functionalization of IONPs were accomplished with facile method simultaneously. This ligand and cross-linking methods have great potential to be applied to the other nanoparticles for improvements of various bio applications.

Blank page

Contents

I. Introduction	10
1.1 General properties of iron oxide nanoparticles (IONPs)	10
1.2 Surface modification of IONPs	12
1.3 Colloidal stability of IONPs	15
1.4 IONPs for bio-applications	18
II. Compact and cross-linked nanoparticles: nano-platform for highly stable, versatile conjugation and its bio-application.	19
2.1 Introduction	19
2.2 Materials & Experimental methods	21
2.2.1 Materials	21
2.2.2 Instrumental and analysis	21
2.2.3 Synthesis of iron-oleate complex	21
2.2.4 Synthesis of iron oxide nanoparticles	21
2.2.5 Synthesis of ligand by RAFT polymerization	22
2.2.6 Ligand exchange of 12 nm IONPs	22
2.2.7 Cross linking of IONPs (CLNPs)	22
2.2.8 Conjugation of rhodamine B isocyanate to CLNPs	23
2.2.9 Synthesis of maleimide propionic acid	23
2.2.10 Conjugation of mannose	23
2.2.11 Conjugation of folic acid	23
2.2.12 MR relaxivity	24
2.2.13 Cell culture	24
2.2.14 Prussian blue staining	24
2.3 Results & Discussion	25
2.3.1 Synthesis of ligand & water dispersible IONPs	25
2.3.2 Cross linking with various diamines	32
2.3.3 Confirmation of cross linked IONPs (CLNPs)	42
2.3.4 Various stability test of CLNPs	46
2.3.5 Multifunctional conjugation of CLNPs	52
2.3.6 Specific targeting test by MR relaxivity	58
2.3.7 In vitro test with folic acid conjugated CLNPs	61
2.4 Conclusion	64

List of Figures

Figure 1. Role of the magnetic nanoparticles as platform materials to be used in bio-application

Figure 2. TEM image of (a) encapsulated NaGdF₄ nanoparticles. (b) silica coated IONPs. (c) IONPs ligand exchanged with water dispersible zwitterionic dopamine sulfonate monomer. (d) IONPs ligand exchanged with multidentate catechol based PEG oligomers.

Figure 3. Scheme of (a) poly(TMSMA-r-PEGMA-r-NAS) (top), carboxyl TCL-SPION showing crosslinking between polymer layers after heat treatment (bottom). (b) cross-linked magnetic nanoparticles after cross-linking between PSI-g-PEG-C12 layers with hexamethylenediamine (HMD).

Figure 4. TEM image of IONPs (a) before ligand exchange and (b) after ligand exchange. (c) DLS data of the IONPs after ligand exchange and purification step.

Figure 5. DLS data after ligand exchange and purification step (a) DP adjustment. (b) ratio control of acrylic acid group. (c) ratio control of DMA the anchor group. (d) camera image of IONPs after click chemistry condition in one week.

Figure 6. NMR data of the optimized ligand (DMA30% Acrylic acid 30% PEG₄₈₀ 40%).

Figure 7. Diamines of various lengths used for cross-linking reaction.

Figure 8. (a) Hydrodynamic diameter (nm) and (b) Zeta potential (mV) values with various diamine additives.

Figure 9. Confirmation of amine functionalized CLNPs with RITC UV-Vis absorbance at wavelength 558 nm (a) ethylene diamine (EDM) (b) Hexamethylene diamine (HDM) and (c) Bis(hexamethylene) triamine (BHTM).

Figure 10. Graph of the calculated number of amine group of each cross-linked nanoparticles (CLNPs).

Figure 11. Camera image of stability test in pH 3 of CLNPs with (a) EDM (c) HDM and (e) BHTM. Their HD sizes in time consuming stability were measured by DLS (b) EDM (d) HDM and (f) BHTM used CLNPs.

Figure 12. Visualization of polymer with 1 wt% of phosphotungstic acid, IONPs polymer by TEM magnification (a) 50 k and (b) 100 k, CLNPs polymer in (c) 50 k and (d) 100 k. (e) DLS data of these extracted polymer.

Figure 13. XPS spectra of C1s peak fitting of (a) IONPs and (b) CLNPs with HDM. N1s peak fitting of (c) IONPs and (d) CLNPs.

Figure 14. Camera image of stability of (a) IONPs-PEG (c) IONPs-AA and (e) CLNPs in wide range of pHs. Graph of hydrodynamic diameter about time consuming results in various pHs (b) IONPs-PEG (d) IONPs-AA and (f) CLNPs.

Figure 15. Camera image of stability of (a) IONPs-PEG (c) IONPs-AA and (e) CLNPs in various concentrations of NaCl solutions. Graph of hydrodynamic diameter about time consuming results in NaCl solutions of (b) IONPs-PEG (d) IONPs-AA and (f) CLNPs.

Figure 16. Stability test in click chemistry conditions with (a) IONPs-PEG (b) CLNPs (c) 24 h later in click chemistry condition IONPs-PEG (left) and CLNPs (right) and (d) measured with DLS. (e) stability test of thermal effect in 95 °C condition. (f) hydrodynamic diameters were measured to observe the effect of purification with viva spin.

Figure 17. DLS data of CLNPs-Man indicates no aggregates while further reactions.

Figure 18. HR-MAS data of CLNP-Man (red), Man-SH (yellow), Polymer ligand (green), and Acetyl protected Man-SH (blue) in D₂O solvent.

Figure 19. FT-IR data of CLNPs (black) and CLNPs-Man (red) to confirm the mannose conjugated CLNPs.

Figure 20. (a) DLS data of after folic acid conjugated to CLNPs (b) UV-Vis absorbance analysis to confirm folic acid conjugation.

Figure 21. Graph of MR T₂ relaxivity (a) with addition of Con A to CLNP (blue) and CLNP-Man (red). (b) changes of T₂ relaxivity of CLNPs-Man using different lectins Con A (red) and WGA (blue).

Figure 22. Microscopy image of Prussian blue stained HeLa cell treated with (a) 200 uM and (c) 500 uM of CLNPs. (b) 200 uM and (d) 500 uM of CLNPs-FA.

List of Tables

Table 1. GPC data of the optimized ligand (DMA30% Acrylic acid 30% PEG₄₈₀ 40%).

Table 2. Hydrodynamic diameter (nm) and zeta potential (mV) values measured by DLS which used various diamines for cross-linking.

List of Schemes

Scheme 1. Scheme of RAFT polymerization.

Scheme 2. Scheme of the optimized ligand for ligand exchange of Fe₃O₄ iron oxide nanoparticles (IONPs) in this research

Scheme 3. Scheme of overall reactions in this research.

Scheme 4. Scheme of the (a) IONPs-AA and (b) CLNPs with 125 eq. of HDM to compare N1s and C1s energy binding peak analyzed by XPS spectra.

Scheme 5. Scheme of multifunctional CLNPs conjugated with (a) mannose and (b) folic acid

Scheme 6. Scheme of CLNPs-Man incubated with Con A resulted in the formation of aggregates, leading to shorter T_2 relaxation time and consequently a darkened MRI image.

Scheme 7. Scheme of folate receptor mediated HeLa cell targeting with CLNPs-FA.

List of Abbreviation

DMA	Dopamine methacrylamide
RAFT	Reversible addition-fragmentationchain trasfer
PEG	Poly(ethylene glycol)
DLS	Dynamic light scattering
FPLC	Fast protein liquid chromatography
AA	Acrylic acid
EDM	Ethylene diamine
HDM	Hexamethylene diamine
BHTM	Bis(hexamethylene) triamine

I. Introduction

1.1 general properties of iron oxide nanoparticles

Iron oxide nanoparticles (IONPs) are superparamagnetic materials, such IONPs have properties of low toxicity and biocompatible. Because of these properties, they have been of great interest in MRI reagent, cell targeting and drug delivery (Figure 1)¹⁻². Especially for bio application of IONPs, synthesize monodisperse nanoparticles were studied in decades³. Highly monodisperse IONPs are essential property in bio application. Because, the size of IONPs affects cellular uptake, and bio distribution when injected in vivo⁴. The size of IONPs should be optimized to avoid rapid excrete by the immune system, and consequently to be accumulated in the target tissue. It was reported that small-sized nanoparticles (e.g., hydrodynamic diameter (HD) of $< \sim 10$ nm) are likely to be excreted. Meanwhile, large particles (e.g., HD of $> \sim 100$ nm) are taken up by phagocytes, and therefore tend to accumulate in tissues. In the case of medium sizes of particles (e.g., HD of 20-100 nm) have long circulation time in body, and they're suitable size to be accumulated through enhanced permeability and retention (EPR) effect to cancer cell vasculature which are hundreds of nanometers⁵. It is well known that the magnetic properties of IONPs depend on the particle size. Unless the IONPs have superparamagnetic characteristics, if there is no external magnetic field, IONPs have no magnetic properties because the magnetic moment of IONPs become randomized by heat energy. However, if the external magnetic field is applied, the magnetic moments of the particles are arranged in a certain direction by the external magnetic field and exhibit strong magnetic behaviors⁶. The IONPs have a surface-to-volume ratio, so the spin canting effect is not negligible. Therefore, the magnetization changes according to the size, which causes T1 and T2 contrast effects⁷.

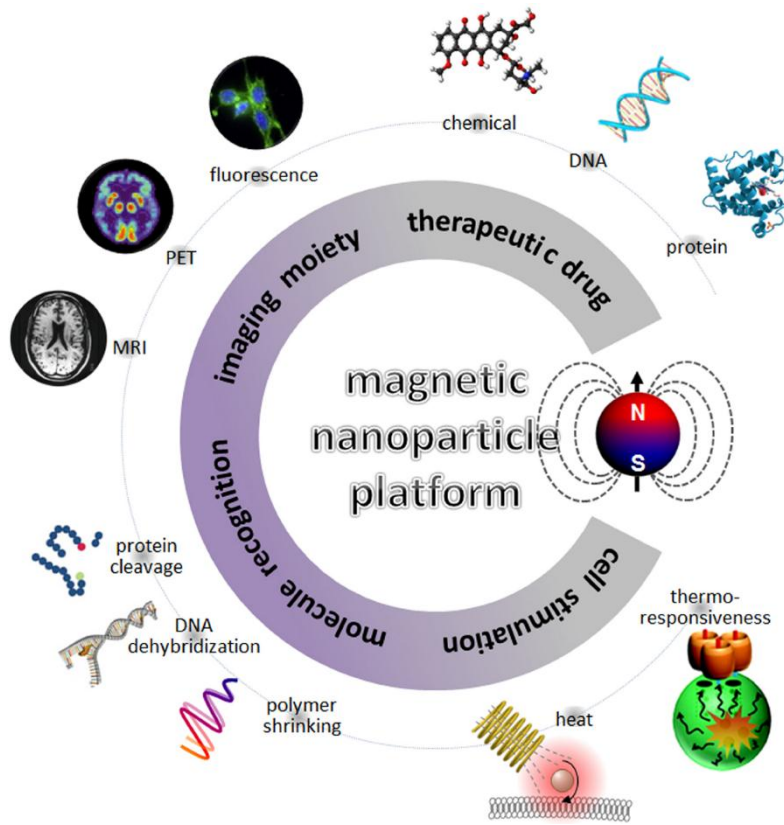


Figure 1. Role of the magnetic nanoparticles as platform materials to be used in bio-application¹

1.2 Surface modification of IONPs

Most effective synthetic process of monodisperse and high quality IONPs is based on high temperature reaction of organometallic precursors. Synthesized IONPs with this approach are mainly dispersed in hydrophobic solvents because they are capping with water-immiscible ligand⁸. Because IONPs are usually applied in bio field, they are required to be dispersed in hydrophilic solvents. To accomplish this requirement, surface modification process of IONPs are necessary, and this surface modification field was researched in many decades. For example, representative surface modification methods are encapsulation⁹, silica coating¹⁰, and ligand exchange¹¹⁻¹³ methods are studied for a long time (Figure 2).

First, the encapsulation method has advantages of simple, reproducible, and rapid without any surface treatment. Individual IONPs could be encapsulated in the hydrophobic core of a micelle composed of a mixture of hydrophobic alkyl chain and poly(ethylene glycol) PEG as a hydrophilic part called polysorbate 80⁹. In addition, PEG is widely used because that is poorly immunogenic and antigenic and acts as excellent repellent for biomolecules. Another research, Johnson, He et al. which used PEGylated phospholipid (DSPE-PEG) micelles to coat NaGdF₄ NCs for bio application¹⁴. Through this approach, they controlled the micellization of NPs, then achieved compact NC-micelles with ultrahigh T_1 relaxivity. On other hand, encapsulation method has limitations of relatively weak colloidal stability in organic solvents, and the purification step of micelles without any NPs is difficult to optimize.

The second most commonly used coating method is silica coating. Silica is well known water soluble and quite biocompatible materials. Owing to these properties, It has a great potential of resist ant to biodegradation, moreover, it can be easily constructive for functionalization of NPs for bioconjugation and targeting in biological systems¹⁵. For example, Lu, Hung et al.¹⁵ developed fluorescein isothiocyanate (FITC) incorporated silica-coated IONPs. However, If NPs surfaces treated with silica coating, the size of IONPs will increased by their thick shell. It may affect lower the MR contrast image because silica coated IONPs have low water access.

To accomplish thin layered, compact, and robust surface modification method, ligand exchange of IONPs were studied in many researches^{12, 16}. Jun, Huh et al¹⁷. used a simple but highly effective 2,3-dimercaptosuccinic acid (DMSA) ligand for IONPs surface modification. The DMSA forms a stable coating through carboxylic bonding and further stabilization is attained through intermolecular disulfide bond between the ligands under ambient conditions. The remaining free thiol groups of DMSA are used for the attachment of target biomolecules. Other approach of ligand exchange method is using phosphine ligand conjugated PEG chain (PO-PEG)¹⁸. The synthesis of PO-PEG is extremely facile, thus it's practical for the large scale preparation of dispersed IONPs. And the last, water soluble zwitterionic dopamine sulfonate ligand was used for surface

modification of hydrophobic IONPs¹⁹. Because dopamine catechol part has a strong binding affinity with surface of IONPs, this property gives IONPs as compact and highly stable in water dispersible conditions by sulfonate group of the zwitterionic ligands. However, even these monomeric ligand exchange methods give highly stable in aqueous media, IONPs required more stability for further reaction such as bio conjugation. To overcome this limitation, the formation of dimer, polymer structures of ligands were used for surface modification^{12,20}. Polymer is consists of several anchor monomers in backbone, this structure enhances probability of ligands to binding IONPs surface. These features improve IONPs colloidal stability in high temperature, and wide range of pH solution.

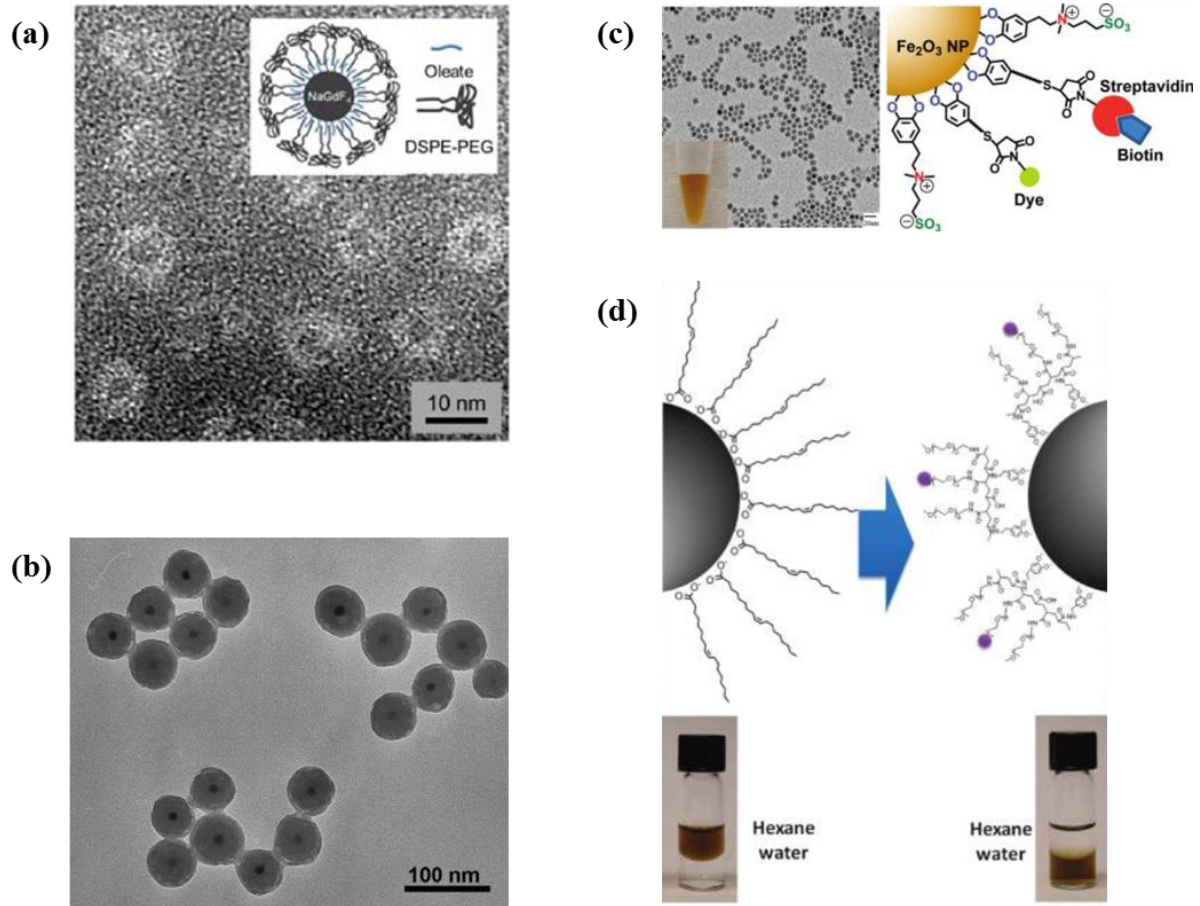


Figure 2. TEM image of (a) encapsulated NaGdF₄ nanoparticles¹⁴. (b) silica coated IONPs¹⁵. (c) IONPs ligand exchanged with water dispersible zwitterionic dopamine sulfonate monomer¹⁹. (d) IONPs ligand exchanged with multidentate catechol based PEG oligomers¹².

1.3 Colloidal stability approaches of IONPs

As NPs are highly increased in applications of chemistry and biology, applications usually require that the IONPs are well dispersed and stable against aggregation in a liquid condition²¹. The relationship between aqueous media and colloidal stable NPs is very important for application in the human body²². As mentioned in several researches, steric and electrostatic repulsion between NPs are essential property for achieving good colloidal stability. Also, good surfactants can provide stabilization of NPs.

To enhance the stability of IONPs in aqueous media, researches tend to modify anchor or spacer group of the water dispersible ligand. Sterically stabilized IONPs are achieved by two general method²², first approach is that dispersants consist of repeated unit with low affinity have possibility of encapsulate several cores together, which derives increase of size. The weak affinity of the stabilizing polymer dispersants reduces iron oxide NP stability²³, protein adsorption to NPs occurred and extremely decreases blood circulation time²⁴. Because the size of NPs become large, the alternative approach is that using with low Mw spacer and high affinity anchor groups which is covalently linked together. In this case, dispersants constructed like brushed structure, NPs stability can be enhanced relatively with compact size. However, these processes have limits of stability in long term, to overcome the limitation ‘cross-linking’ was considered as alternative method.

The cross-linking is that the tight binding of ligands on the surface of NPs to prevent ligand detachment. cross-linked iron oxide nanoparticles (CLIO) had been developed²⁵, and they are composed of chemically cross-linked dextran coated IONPs²⁶. These synthesized CLIOs are considered as the most effective MR contrast agents because of their stable coating, and compact hydrodynamic size²⁷⁻²⁸. Also, cross-linked NPs with biocompatible polymer or dendrimer had been reported²⁹. For example, Jon et al.³⁰ reported thermally cross-linked superparamagnetic iron oxide nanoparticles (TCL-SPION) which cross-linked with thermal reaction of Si-OH containing copolymer unlike chemical cross-linking system³⁰. In this research, they used denoted as poly-(TMSMA-r-PEGMA) random copolymer, it consists of ‘surface anchoring moiety’ (silane group) and a ‘protein-resistant moiety’ (PEG). Highly stable polymer coating was performed, PEG-silane copolymer became cross-linked as hydrolyzation of silane groups (-Si(OH)₃) by simple heat treatment. Furthermore, functionalization of TCL-SPION was performed simultaneously (figure 3a). The other approach for cross-linking was reported by Kim et al.³¹ they developed cross-linked polymeric nano assemblies by cross-linking of poly(succinimide) (PSI) with hexamethylene-dimaine (HMD) linker (figure 3b)³¹, and they were successfully prepared to show strong potential for bio-applications.

Through these cross-linked magnetic nanoparticles were developed to improve the structural

stability of amphiphilic polymer coated magnetic nanoparticles. These nanoparticles show strong potential for biomedical applications

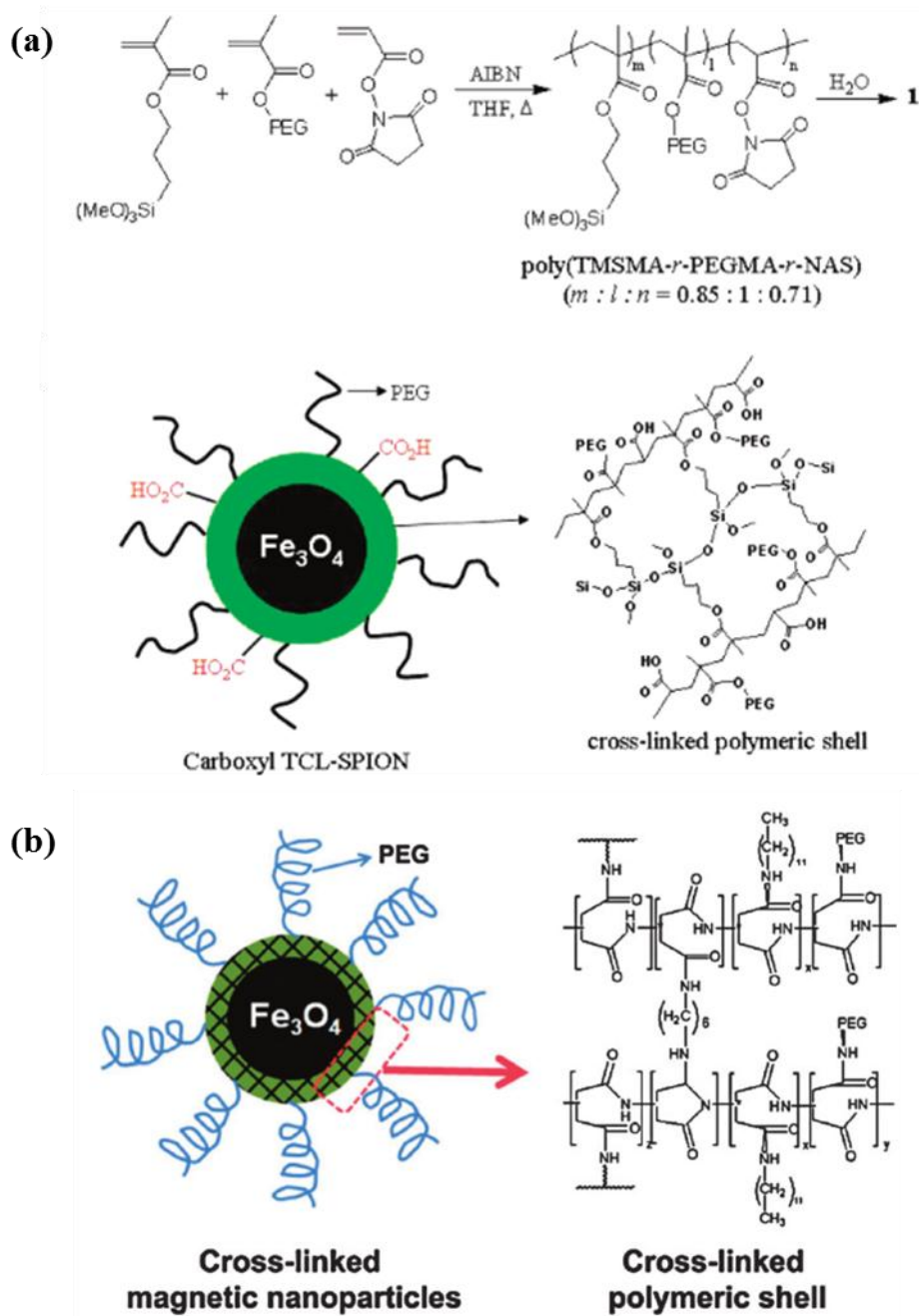


Figure 3. Scheme of (a) poly(TMSMA-*r*-PEGMA-*r*-NAS) (top), carboxyl TCL-SPION showing crosslinking between polymer layers after heat treatment (bottom)³⁰. (b) cross-linked magnetic nanoparticles after cross-linking between PSI-g-PEG-C12 layers with hexamethylenediamine (HMD)³¹

1.4 IONPs in bio application

In bio-application, surface functionalized magnetic iron oxide nanoparticles (IONPs) are a kind of novel functional materials³². The bio-applications of IONPs are known Magnetic resonance imaging (MRI) contrast agents³³⁻³⁵, cancer cell targeting³⁶⁻³⁷, and magneto responsive therapy³⁸⁻³⁹ (figure 1)¹.

IONPs are the most appropriate substances which can be alternative MRI contrast agents because of their high biocompatibility. To obtain a magnetic resonance signal, IONPs are placed in a strong magnetic field (B_0). When a resonant radiofrequency is irradiated, the nucleus absorbs the energy and the number of the spins with a higher-energy state increase^{25, 40}. Then, the nuclei return to the equilibrium state, it is referred to as relaxation. There are two types of relaxation processes, The T_1 relaxation time represents the time required for longitudinal magnetization to recover from zero to a value of 63% of the original state. The T_2 relaxation time represents the time for the transverse magnetization to drop from the maximum to a value of 37% of its excited state⁴¹. Although IONPs affect both the longitudinal and transverse relaxation processes, they're mostly used in T_2 relaxation. Because the T_2 contrast effect is highly dependent on the magnetization of a particle, the r_2 values can be increased by enhancing the magnetic moment of a nanoparticle or clustering of nanoparticles^{1, 41-42}.

There have been many studies on cancer cell targeting using IONPs⁴³⁻⁴⁶. There are two approaches in cancer cell targeting, one is active targeting and the other is passive targeting. First, the passive targeting is processed with EPR effect when nano sized up to 100 nm of NPs were used. This phenomenon is caused by accumulation of leaky vasculature of tumor cell⁴⁷. However, NPs large size of NPs are hard to penetrate into the dense tissue matrix. To overcome this limit, Wong, Stylianopoulos et al.⁴⁷ introduced multistage nanoparticles concept to IONPs of passive targeting. 100 nm nanoparticles separate to 10 nm nanoparticles after they excrete from leaky vasculature of the tumor. Another approach of targeting is the active targeting which requires bio molecules such as glucose or folic acid of targeting reagent. Immobilized targeting ligand recognizes receptors over expressed on the exterior surface of cancer cells⁴⁸. G. Chen et al. reported the development of magnetic and folate (FA)-modified cell-derived microvesicles (MVs) which exhibited significantly enhanced antitumor efficacy both in vitro and in vivo⁴⁶. It indicates active targeting method is available to selective uptake and better distribution in the tumor cell.

II. Compact and cross-linked nanoparticles: nano platform for highly stable, versatile conjugation and its bio-application.

2.1 Introduction

Superparamagnetic iron oxide nanoparticles (IONPs) have great potential in bio application because of their adequate properties for bio media such as low toxicity and biocompatibility²². In addition, they have been researched in various field for decades, for example, magnetic resonance imaging (MRI)^{6, 41-42, 49}, drug delivery^{1, 50}, cell labeling^{4, 51}, separation^{43, 52}, tracking⁵³, and hyperthermia⁵⁴. For IONPs in these representative bio applications, monodisperse, good dispersity, low toxicity and colloidal stability properties are required in biological media⁴¹. In previous researches, it has been widely known to synthesize high quality of metal oxide with uniformity and crystallinity in organic solvent³. However, as these highly monodisperse nanoparticles are composed of hydrophobic ligand, it is difficult to disperse in the water and bio application is not possible. Therefore, surface modification of nanoparticles (NPs) is essential. There have been various surface modification methods for water-dispersible NPs^{4, 46, 51}. The most commonly used methods are silica coating⁵⁵, encapsulation⁵⁶, and ligand exchange⁵⁷. Although water-dispersible, stable, and biocompatible NPs are synthesized through these facile modification methods, these NPs formed as large sizes because of their thick shell coating, also, there are limits such as low surface coating yield, low reproducibility and stability. Since the colloidal stability is a most important issue in bio-applications, high stability is the most required factor. To be used in bio media, NPs should be stable enough to withstand wide range of pHs, stain in nonspecific binding by protein, and long circulation in human body.

In order to satisfy both of these limitations and requirements, a ‘Cross-linking’ method was introduced into the water-dispersible NPs. Cross-linking is simply a way to tightly ligate the ligands on the surface of NPs.^{31, 53, 58} In previous research, cross linked iron oxide nanoparticles (CLIO) using dextran was developed before, these are used in T_2 MRI agent because they are biocompatible, and relatively monodisperse. However, because they’re synthesized with co-precipitation method, they have low contrast effect. Also, they must be functionalized through a complicated process with chemical reaction which has toxicity in vivo system. To overcome these limitations, cross-linking system was applied to the monodisperse IONPs ligand exchanged with biodegradable polymers. Recently, IONPs modified with poly(succinimide) (PSI) were cross-linked with hexamethylenediamine (HMD) research was reported, although they’re stable and biocompatible, the 12 nm of cross-linked IONPs size was increased to 45 nm, and they have low reproducibility. In advance of cross-linking aspects, there was no significant evaluation factors and confirmation

of cross-linked nanoparticles.

In this research, a polymer ligand was optimized by RAFT polymerization for compact and robust water dispersible IONPs, and cross-linking reaction was proceeded with diamine and carboxyl on surface was conjugated by EDC coupling reaction. Furthermore, studied effect of cross-linking by using different lengths of diamines and various addition equivalents. To confirm cross-linked nanoparticles, XPS spectra was used and visualization of CLNPs was attempted by TEM analysis with negative staining method. Moreover, highly enhanced stability of CLNPs were performed by wide range of pHs and NaCl, temperature effect, purification step and 'click chemistry' condition which is known as harsh environments for NPs. At the same time, with diamine cross-linking process, the amine group expected to be functionalized on CLNPs surface. Through confirmation of free amine group of CLNPs, bio molecule conjugate experiments were performed using mannose and folic acid. To confirm conjugation of bio molecules, HR-MAS, FT-IR, and UV-Vis were analyzed. Finally, to evaluate their bio abilities were retained after CLNPs conjugation, MR relaxivity measure and in vitro test were performed. Through these results, the highly stable and multifunctional nanoparticles were synthesized through facile diamine conjugation of IONPs. This cross-linking platform has great potential in application of other NPs.

2.2 Experimental methods

2.2.1 Materials

Iron chloride, sodium oleate, oleic acid, 1-octadecene, acrylic acid, poly(ethylene glycol) methyl ether acrylate, 2-(2-aminoethoxy) ethanol (AEE), 1-ethyl-3-(3-dimethylaminopropyl) carbodiimide hydrochloride (EDC) were purchased from Sigma-Aldrich. N-hydroxysulfosuccinimide (sulfo-NHS) was purchased from TCI. 10x phosphate buffer saline was purchased from Biosesang. Dopamine methacrylamide were synthesized as previously reported⁵⁹.

2.2.2 Instrumental and analysis

¹H NMR spectra were recorded using a 400 MHz Bruker spectrometer. Residual proton signal of deuterated solvent was selected as the reference standard. The HR-MAS proton spectra were recorded on a 700MHz FT-NMR Spectrometer (Western Seoul Center, Korea Basic Science Institute). The Size and morphologies of nanoparticles were studied by transmission electron microscopy (TEM, JEOL, JEM-2100) which was operated at 200 kV. Dynamic light scattering (DLS) measurements were performed on a Malvern Instruments Zetasizer Nano-ZS90 at 25 °C. Gel Permeation Chromatography (GPC, Shimadzu, eluent; THF) was used for measure molecular weight of synthesized polymer. X-ray photoelectron spectroscopy (XPS) spectra were performed in UCRF. UV-Vis spectra (Shimadzu UV-1800) were taken with a quartz cuvette. Infrared (IR, Varian 670/620) were measured at room temperature with Ar inert atmosphere. Magnetic relaxivity was measured with minispec (Bruker) at 37 °C. For purification of excess ligand or molecules, fast protein liquid chromatography (FPLC, GE healthcare) and G-25 sephadex column were used.

2.2.3 Synthesis of iron-oleate complex

The metal-oleate complex was prepared by reacting metal chlorides and sodium oleate. To synthesize iron-oleate complex, 5.4 g of iron chloride (FeCl₃·6H₂O, 20 mmol) and 18.3 g of sodium oleate (60 mmol) was dissolved in a mixture solvent composed of 40 ml ethanol, 30 ml distilled water and 70 ml hexane. The resulting solution was heated to 70 °C and kept at that temperature for 4 hours. When the reaction was completed, the upper organic layer containing the iron-oleate complex was washed at least 3 times with 15 ml distilled water and 10 ml ethanol solvent in a separatory funnel. Resulting in iron-oleate complex in a waxy solid form.

2.2.4 Synthesis of iron oxide nanocrystals

The following procedure is optimized for synthesis of monodisperse iron oxide (magnetite) nanocrystals with 12 nm particle size. 0.9 g (1 mmol) of the iron-oleate complex synthesized as described and 0.2 g of oleic acid (0.73 mmol) were dissolved in 1.5 g of 1-octadecene (90%) at

room temperature for 1 hour. The reaction mixture was heated to 320 °C with a constant heating rate of 3.3 °C min⁻¹ in Ar inert atmosphere, and then aging the mixture at that temperature for 30 min. After the reaction is over, the solution containing the nanocrystals was then cooled to room temperature with Ar purging. To get the solution to precipitate the nanocrystals, acetone:ethanol 3:1 solvent was added. The nanocrystals can be separated by centrifugation.

2.2.5 Synthesis of ligand by RAFT polymerization

To synthesize the ligand we used RAFT polymerization method. 0.13 g of dopamine methacryl amide (0.6 mmol), 0.04 g of acrylic acid (0.6 mmol) and 0.4 g of poly(ethylene glycol)₄₈₀ (0.8 mmol) were dissolved in dimethylformamide (DMF). 0.03 g of dibenzyl trithiocarbonate RAFT agent (0.1 mmol) was prepared. To afford a controlled living polymerization, 8 mg of radical initiator agent azobis(2-cyanopentanoic acid) AIBN was added (0.05 mmol). The mixtures of monomers transferred to the 4 ml ampule. The ampule was subjected to 3 cycles of freeze-pump-thaw, and sealed under vacuum condition using a torch. The ampule was heated to 70 °C on an oil bath for overnight. After the reaction is over, synthesized polymer was washed with diethyl ether (Aldrich, 99.5%) to remove unreacted monomers. Excess solvent was dried under vacuum oven for 12 hours.

2.2.6 Ligand exchange of 12 nm IONPs

Ligand exchange was carried out in a 5 ml vial. Prepare 10 mg of 12 nm IONPs dispersed in 1 ml of tetrahydrofuran (THF) solvent. 0.04 g of polymerized ligand (0.05 mmol), and 0.2 g of coating reagent 2-(2-aminoethoxy) ethanol (0.95 mmol) were mixed together with prepared THF dispersed IONPs in 5 ml vial. The ligand exchange reaction was heated to 60 °C on an oil bath for 12 hours. The product was washed with diethyl ether in 50 ml falcon tube, then the precipitates were obtained by centrifugation. Excess solvent was removed in vacuum oven, then dispersed in 1xPBS. The excess ligand and CR reagent were purified by fast protein liquid chromatography (FPLC) G-25 sephadex column.

2.2.7 Cross linking of IONPs (CLNPs)

Cross linking reaction was achieved through amide bond by EDC/Sulfo-NHS reaction with carboxyl group on the IONPs surface using diamine. The amount of diamine added was set at various ratios to the carboxyl group on the surface. The reaction was held in the total IONPs concentration was set to 0.3 mM. EDC/Sulfo-NHS pre-activation step of water dispersed IONPs was held about 1 hr in thermos mixer 1000 rpm, then several ratios of diamine dissolved in water

was added. The total reaction volume was 1 ml. After the reaction, excess EDC/Sulfo-NHS and diamine were removed by viva spin cut off 50k.

2.2.8 Conjugation of rhodamine B isocyanate to CLNPs

To quantify the number of functionalized amine group of CLNPs, we used RITC conjugation and analyzed by UV-Vis absorbance. Prepare CLNPs dispersed in pH 9 buffer solution, then RITC dissolved in DMSO solution was added as 1 equivalent of the expected carboxyl group on the CLNPs surface.

2.2.9 Synthesis of maleimide propionic acid

To synthesize the linker maleimide propionic acid, add 2.699 g of β -alanine (30.3 mmol) into 2.903 g of maleic anhydride (29.6 mmol) dissolved DMF solution. The mixture was stirred for 2 hr at RT. Lower the temperature of the mixture to 0 °C with ice bath. Add 4.255 g of NHS (37 mmol) and 12.98 g of DCC (63 mmol) to the mixture, then stirred at RT vigorously overnight. Filtered white precipitates then evaporates solvents totally. Dissolve the product in DCM, extract the product with DI water. Concentrate the product with evaporator and purify it with column.

2.2.10 Conjugation of mannose

Disperse amine functionalized CLNPs in 250 ul of DMF solution. Add DMF dissolved maleimide propionic acid as 1 equivalent ratio relative to amine group of CLNPs. Total reaction volume was 500 ul in micro tube, react with thermo mixer 4 hrs. add the 1 equivalent of acetyl protected mannose was dissolved in 250 ul of DMF to the mixture for overnight at RT. To make basic condition, add 10 ul of triethylamine. To purify excess maleimide propionic acid linker and mannose, dialysis process in pH 11 buffer solution was required. At the same time, DMF solvent was exchanged with pH 11 buffer and acetyl group was deprotected.

2.2.11 Conjugation of folic acid

To conjugate folic acid to amine functionalized CLNPs, prepare 1 equivalent ratio of folic acid relative to concentration of CLNPs in 1xPBS (pH 7.4) solution. Pre-activation of folic acid was proceeded with excess amount of EDC/Sulfo-NHS for 1 hr. CLNPs dispersed in 1xPBS were added into activated folic acid solution, the reaction was taken for overnight at RT. To purify excess

reagents, FPLC (sephadex G-25) was used.

2.2.12 MR relaxivity

To measure the relaxivity of CLNPs-Man, concentration of 0.6 uM CLNPs-Man were prepared. The sample was prepared total volume of 300 ul and volume of additive Con A (0.01 mg/ul) was set as 0, 10, 30, 50, 100 ul. CLNPs-Man sample and Con A solution were mixed in T-tube for 1 min then transferred to the MR relaxivity analysis tube. Same procedure was applied to IONPs.

2.2.13 Cell culture and preparation

HeLa cells are cultured in using DMEM media supplemented with 10% Tet approved FBS and 1X pen/strep, wash cells with PBS buffer 1 time and add 2 ml of Tryple solution to the cells. Then incubate HeLa cells for 2 min at 37°C. Then add 5 ml of complete media to the HeLa cell solution. Finally replate cells at a 1:20 dilution in 24 well plates.

2.2.14 Prussian blue staining

HeLa cell lines were incubated in 12-well plate. CLNPs-FA were treated in HeLa cell a final concentration of 200 and 500 µg/mL per well. After 6 hr, cells were washed three times with PBS solution, then CLNPs conjugated HeLa cells were treated with 0.5 ml of 10% formalin solution for 5 min to fixation step, and then washed with PBS. Prussian blue staining was then performed. To each well was added a 1:1 mixture of 4% potassium ferrocyanide(II) trihydrate and 2% HCl solution (0.5 mL), and cells were incubated for 15 min, counterstained with nuclear fast red for 3 min, and then washed 2 times with PBS.

2.3 Results & Discussion

2.3.1 Synthesis of ligand & water dispersible IONPs

Iron oxide nanoparticles (IONPs) of uniform size (12 nm) are synthesized as previously reported³ (figure 4a), IONPs are capped with a hydrophobic ligand because they are synthesized in the oil phase. Hydrophilic properties are required for bio-application of IONPs. To impart hydrophilic properties to the IONPs, we used compact and robust ligand exchange method. The ligand used in this research was synthesized as random copolymer through RAFT polymerization (scheme 1). To design appropriate polymer for water dispersible IONPs, dopamine methacrylamide (DMA) was used as an anchor group binding to the surface of IONPs, poly(ethylene glycol) (PEG mw. 480) was used as hydrophilic chain part, and the carboxyl functional group was obtained by adding acrylic acid monomers. To optimize the composition of these ligands, length of ligand, ratio of carboxyl group and anchor group (DMA) were considered while polymerization. Each polymer synthesized under these conditions was characterized by gel permeation chromatography (GPC) and nuclear magnetic resonance (NMR). To determine if the exchanged ligand was suitable, we measured particle size changes with dynamic light scattering (DLS) (figure 5).

First, as polymer DP were set to 20, 50, and 100, it was expected that polymer would cover IONPs as the length became longer. However, IONPs were aggregated as the length became longer. This result is due to the stability of the IONPs decreased due to the interaction between fast protein liquid chromatography (FPLC) column during purification process when long polymer is used (figure 5a). As a result, polymer DP was fixed at 20 as normally it was. The ratio of carboxyl group added to the ligand was set to 10, 20, and 30%, then observed size change of IONPs after ligand exchange. As a result, the stability of the particles was found to decrease as the ratio of carboxyl group decreased (figure 5b). This is because the negative charge ratio of carboxyl is increased and charge repulsion is formed, which makes more stable in water dispersion. Also, partial of carboxylic acid tends to bind to the surface of IONPs that helped the ligand to be attached better to IONPs. Finally, the stability of the IONPs was confirmed by increasing the anchor group, DMA addition ratio to 30, 40, and 50%. As the result of DLS measurement, it was observed that compact size was maintained under all conditions (figure 5c). For further comparison of these results, we confirmed the stability of each ligand exchanged IONPs in a harsh 'click' chemistry condition (Figure 5d). As a result, DMA 30% PEG₄₈₀ 40% Acrylic acid 30% ligand exchanged IONPs did not become degradation and were stable even after 1 week. This is because the hydrophilic and acid functional parts were polymerized in an appropriate rate. Therefore, the optimal ligand composition to be used in this research is DMA 30% PEG₄₈₀ 40% Acrylic acid 30% (scheme 2).

When the ligand exchange was performed using the optimized ligand, the absence of aggregation was confirmed by transmission electron microscopy (TEM) (figure 4b) and DLS (figure 4c). This compact and robust water dispersible IONPs have been synthesized, but still need to be supplemented with stability.

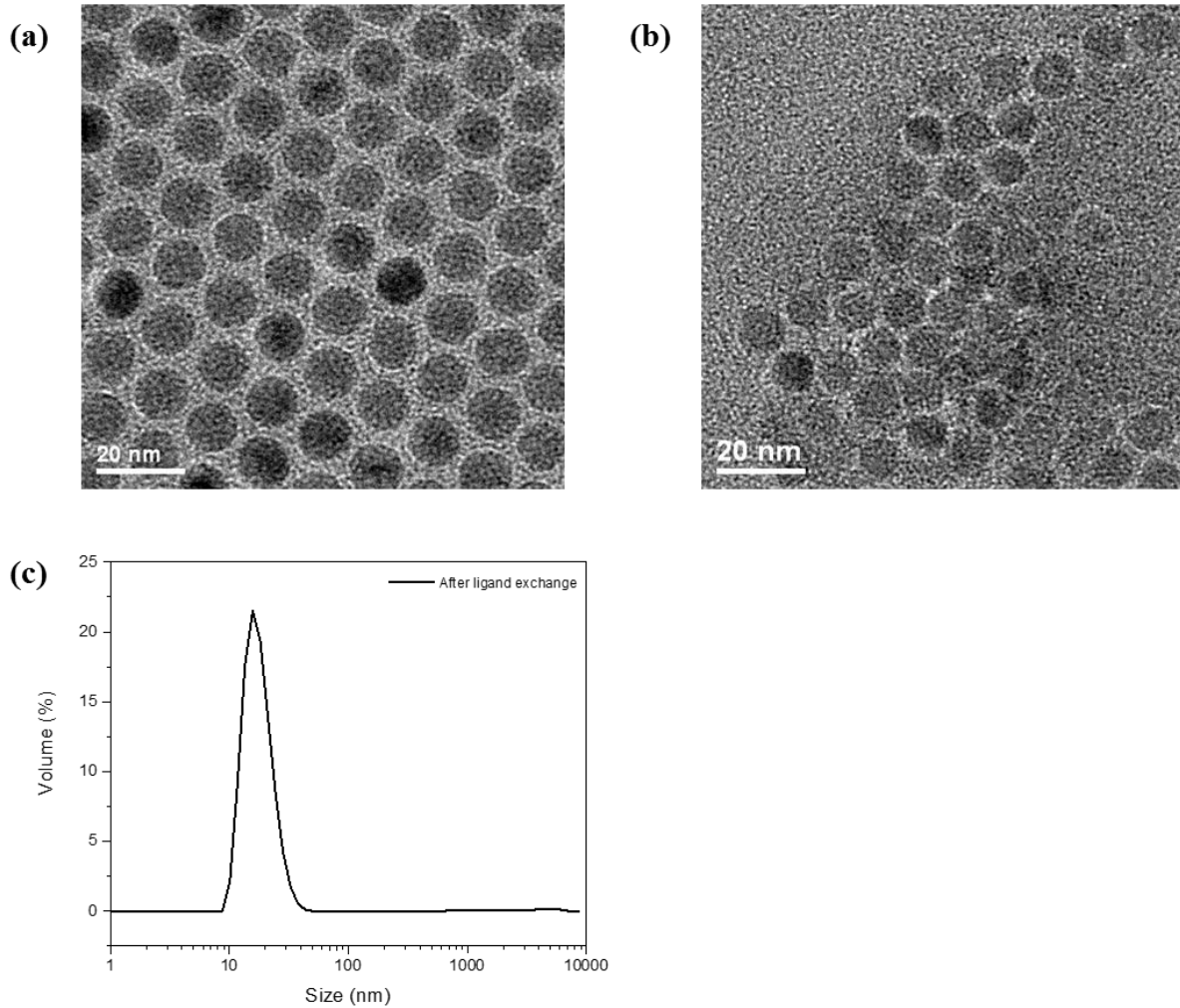
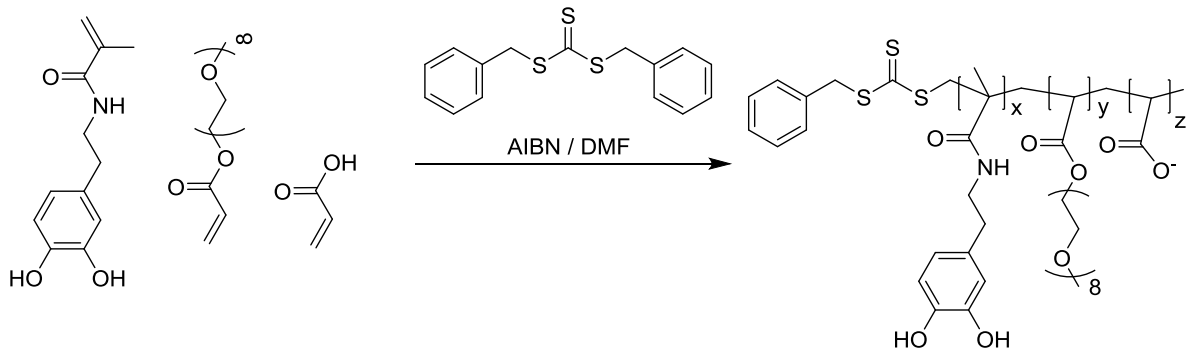


Figure 4. TEM image of IONPs (a) before ligand exchange and (b) after ligand exchange. (c) DLS data of the IONPs after ligand exchange and purification step.



Scheme 1. Scheme of RAFT polymerization.

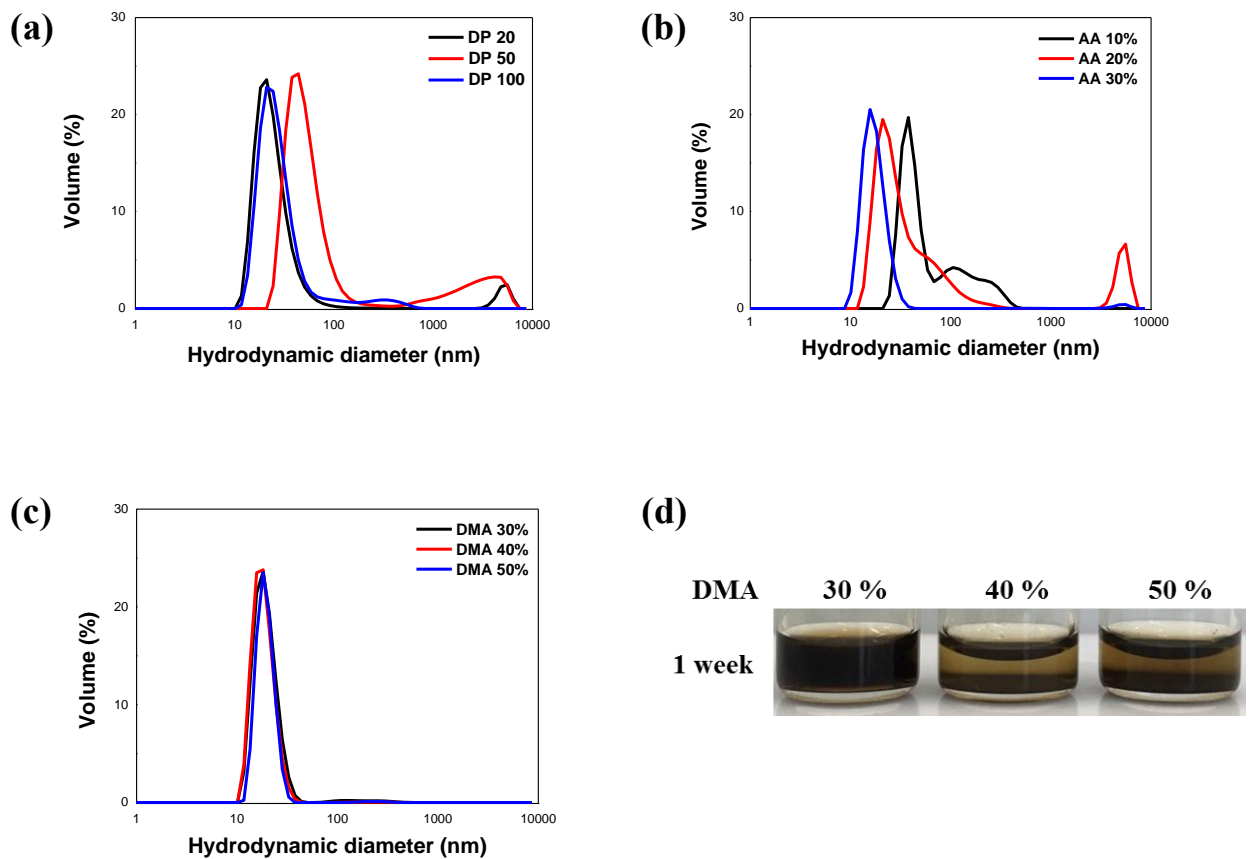
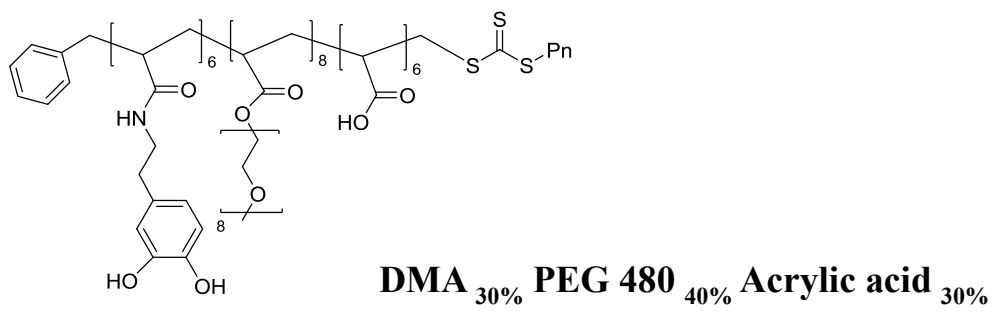


Figure 5. DLS data after ligand exchange and purification step (a) DP adjustment. (b) ratio control of acrylic acid group. (c) ratio control of DMA the anchor group. (d) camera image of IONPs after click chemistry condition in one week.



Scheme 2. Scheme of the optimized ligand for ligand exchange of Fe₃O₄ iron oxide nanoparticles (IONPs) in this research

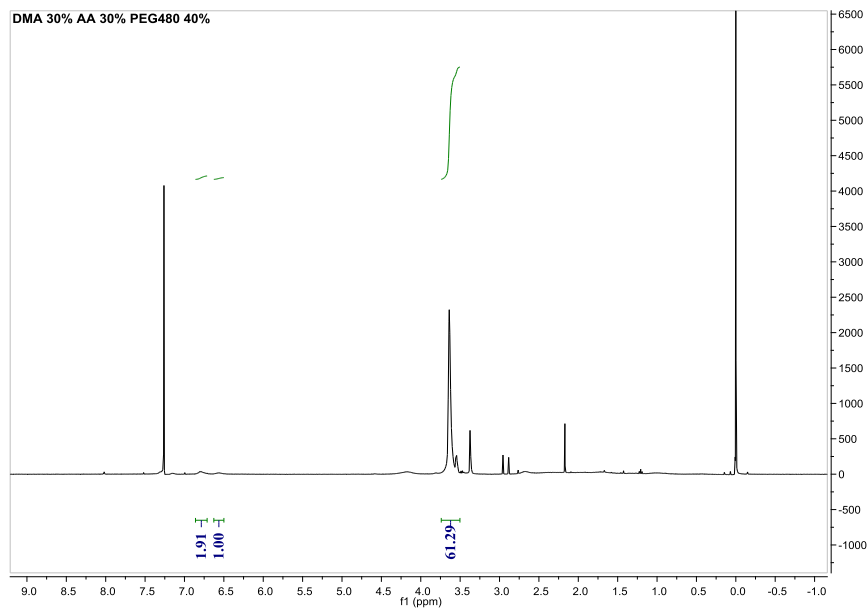


Figure 6. NMR data of the optimized ligand (DMA30% Acrylic acid 30% PEG₄₈₀ 40%).

Mw	Mn	PDI (Mw/Mn)
4668	3967	1.17

Table 1. GPC data of the optimized ligand (DMA30% Acrylic acid 30% PEG₄₈₀ 40%).

2.3.2 Cross linking with various diamines

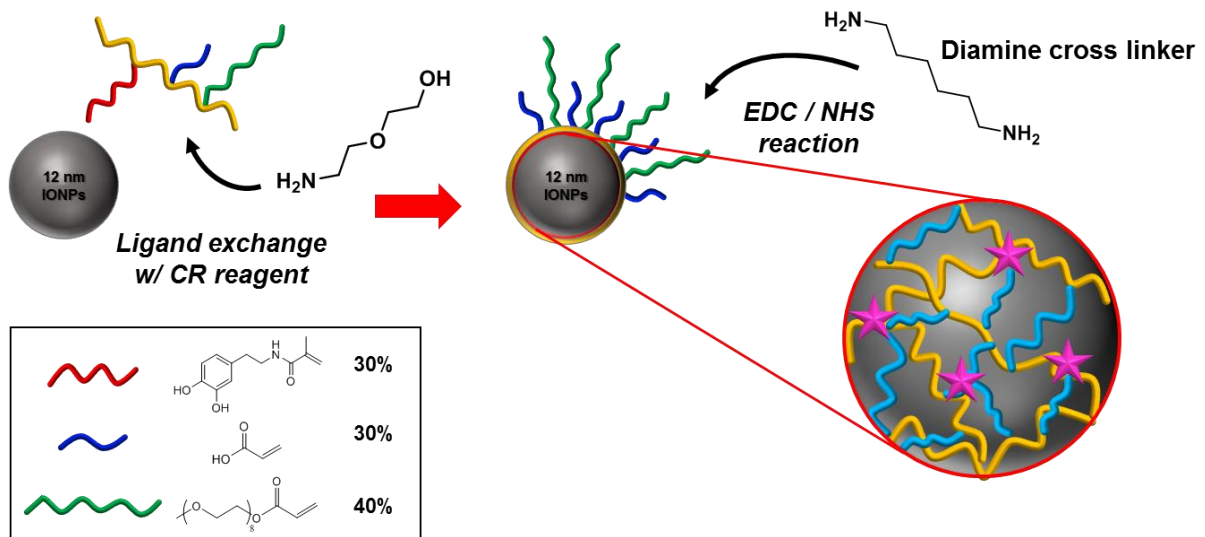
Various bio-molecule conjugation and purification steps are essential for the application of water dispersible IONPs to bio-fields. Since the chemical reaction process is inevitable in the conjugation process, IONPs may be unstable at this part. To overcome this limitation, we enhanced the stability of ligand exchanged IONPs with cross-linking the surface ligands by EDC coupling with diamine (scheme 3).

In this research, three diamines used for cross-linking, ethylene diamine (EDM), hexamethylene-diamine (HDM), and Bis(hexamethylene) triamine (BHTM) were selected to compare the colloidal stability and expression level of amine functional group of cross-linked IONPs (CLNPs) (figure 7). First, IONPs surface activation was performed by setting the amount of 1-ethyl-3-(3-dimethylaminopropyl) carbodiimide hydrochloride (EDC) and N-hydroxysulfosuccinimide (sulfo-NHS) to be compared with the expected amount of carboxyl group on the surface of 12 nm IONPs that had been modified with optimized ligand. The amount of diamine added was summarized (table 2, figure 8). The reason why the amount of diamine added to IONPs was set to at least 125 equivalents (eq.) is when the diamine was added above 100eq. of carboxyl group, there was no enhancement in colloidal stability. After cross-linking reaction, hydrodynamic diameter (HD) of CLNPs were measured with DLS to confirm the size of the CLNPs were maintained after reaction. As shown in the Table #, all the diamine conditions maintain compact HD CLNP size ($\sim 25 \pm 5$ nm). Also, analysis of zeta potential of CLNPs were required to compare extent of cross-linking reaction by various concentrations of diamines. As a result, the zeta potential value of CLNPs with hexamethylene diamine was found to be the least neutral ($\sim -19 \pm 2$ mV) because the carboxyl group and both amine was coupled well, so it means that cross linking with HDM has been done well in this condition. On the other hand, in the other diamine conditions, the CLNPs charges were found to be quite neutral. The reason for this is presumably because the diamine is not used for all cross-linking, and one amine moiety have been expressed.

To approve the assume that the HDM was well conjugated as cross-linking reagent, and the others are suitable for functionalization of amine group, the number of functionalized amine group in CLNPs was calculated by rhodamine B isocyanate (RITC) conjugation. RITC dye can be detected by UV-Vis spectroscopy, it has absorbance at wavelength 558 nm, then the conjugated RITC can be calculated by integrating the normalized UV graph (figure 9). First, cross-linked with HDM, it shows the lowest number of accessible amine (figure 10). This can be interpreted as both amine of HDM was well conjugated to carboxyl group of the surface. Unlike this result, the other diamines show increased number of amines compared to HDM.

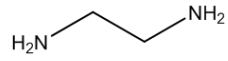
To confirm that cross-linked using HDM enhanced stability of CLNPs, we observed colloidal

stability test of each diamine cross-linked conditions in pH 3 buffer solution (figure 11). As shown in the camera image, it seems to be maintain stable in all diamine conditions for 1 week. However, the size distribution of each CLNPs measured by DLS, interprets that CLNPs are stable under most conditions except cross-linked with 125 eq. of ED. The highly stable CLNPs were cross-linked with 250 eq. of HDM. Through these results, diamine cross-linking which enhances the stability of the IONPs was ensured and the amine functionalization could be achieved simultaneously.

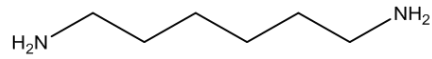


Scheme 3. Scheme of overall reactions in this research.

Ethylenediamine



Hexamethylenediamine



Bis(hexamethylene)triamine

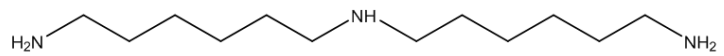


Figure 7. Diamines of various lengths used for cross-linking reaction.

		w/o cross linking	125 eq.	250 eq.	500 eq.	1000 eq.
Ethylene diamine	HD (nm)	17.8	17.77	17.96	16.15	21.56
	Zeta potential (mV)	-35.9	-3.56	-1.18	-1.30	-1.58
Hexamethylene diamine	HD (nm)	17.8	19.7	19.60	19.76	19.90
	Zeta potential (mV)	-35.9	-19.3	-19.5	-18.8	-17.2
Bis(hexamethylene) triamine	HD (nm)	17.8	17.45	17.05	18.48	20.1
	Zeta potential (mV)	-35.9	-7.54	-8.87	-18.8	-4.54

Table 2. Hydrodynamic diameter (nm) and zeta potential (mV) values measured by DLS which used various diamines for cross-linking.

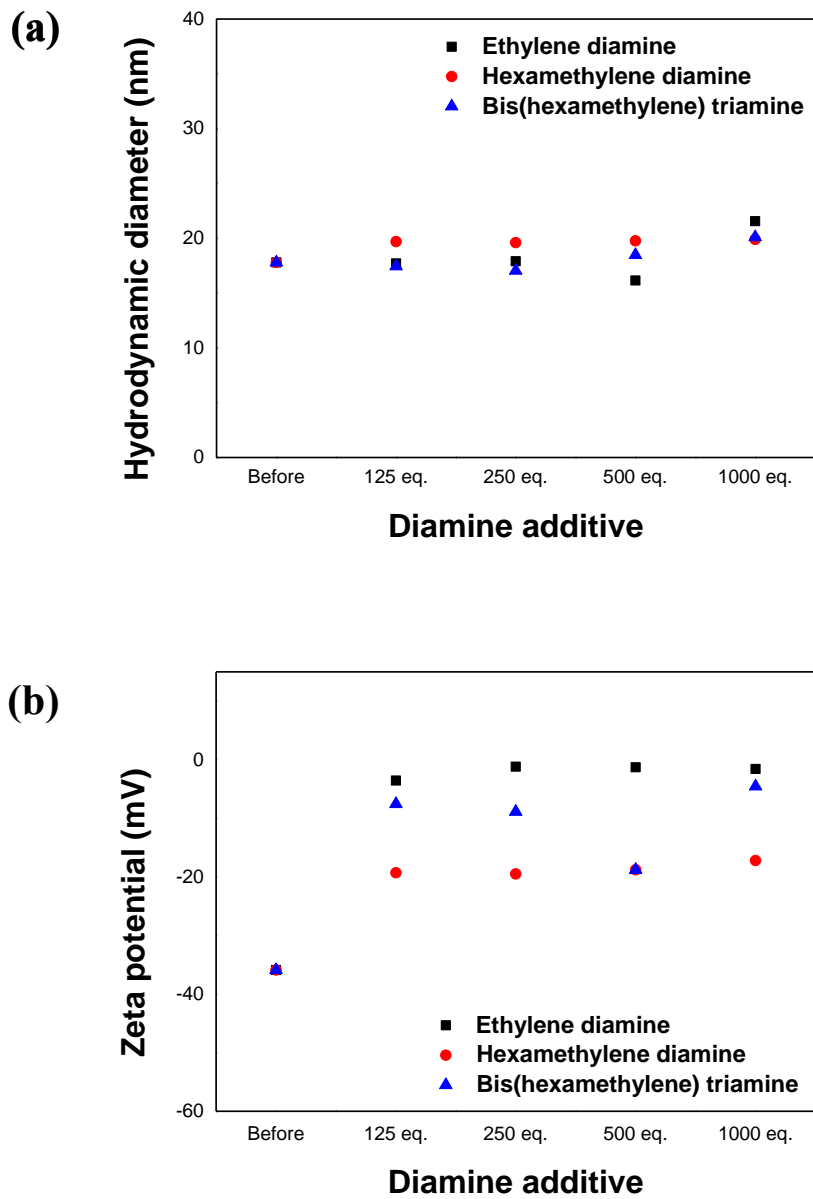


Figure 8. (a) Hydrodynamic diameter (nm) and (b) Zeta potential (mV) values with various diamine additives.

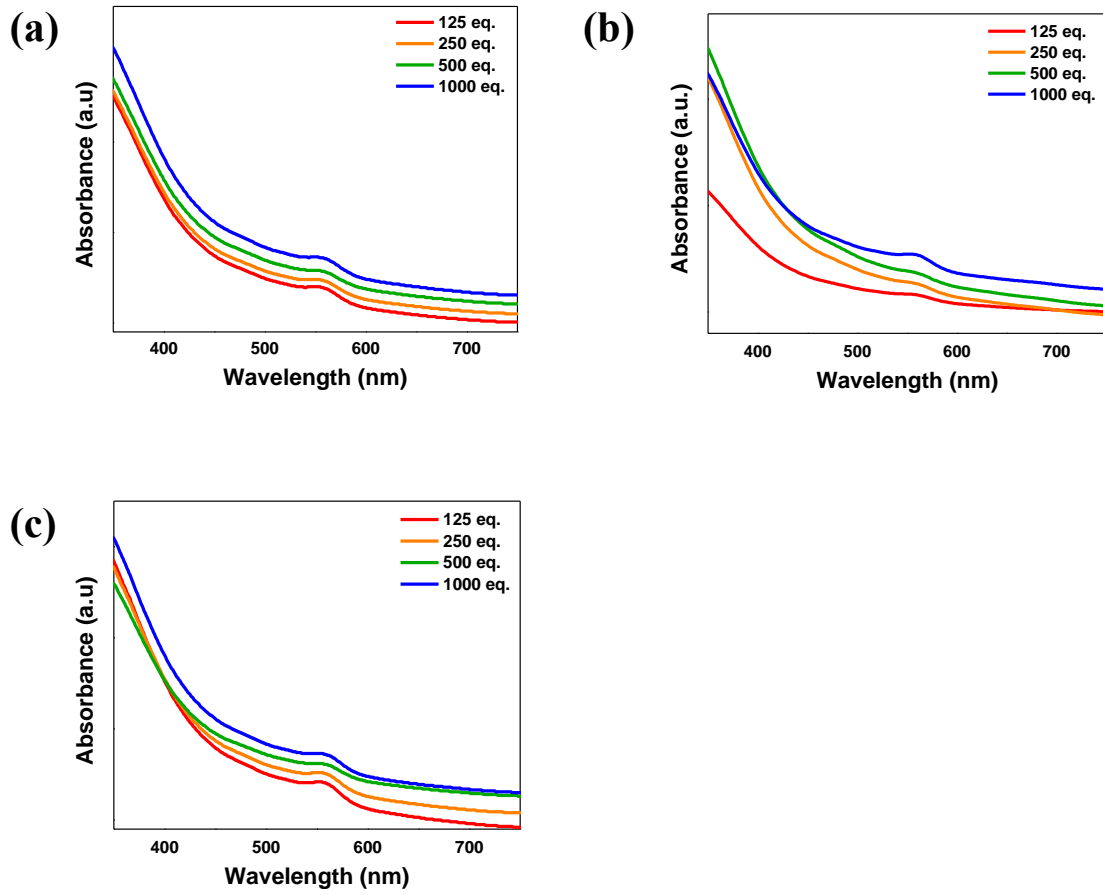


Figure 9. Confirmation of amine functionalized CLNPs with RITC UV-Vis absorbance at wavelength 558 nm (a) ethylene diamine (EDM) (b) Hexamethylene diamine (HDM) and (c) Bis(hexamethylene) triamine (BHTM).

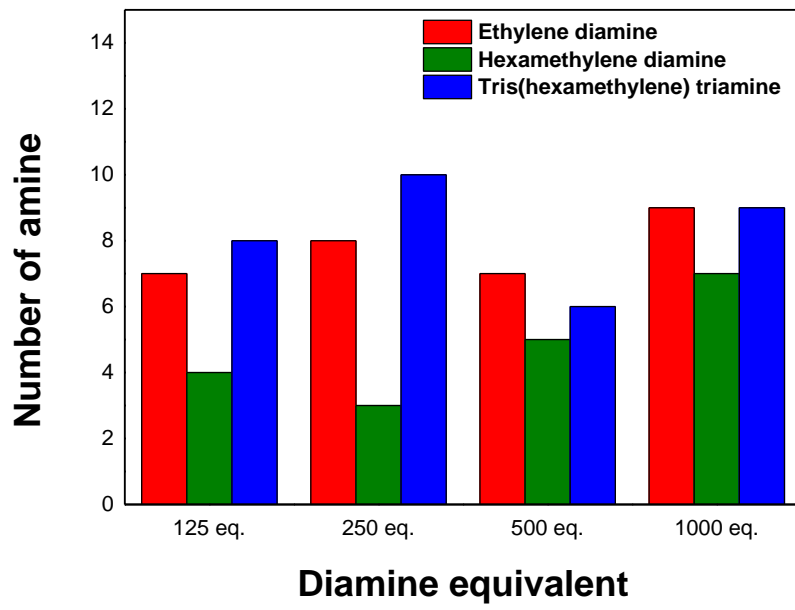


Figure 10. Graph of the calculated number of amine group of each cross-linked nanoparticles (CLNPs).

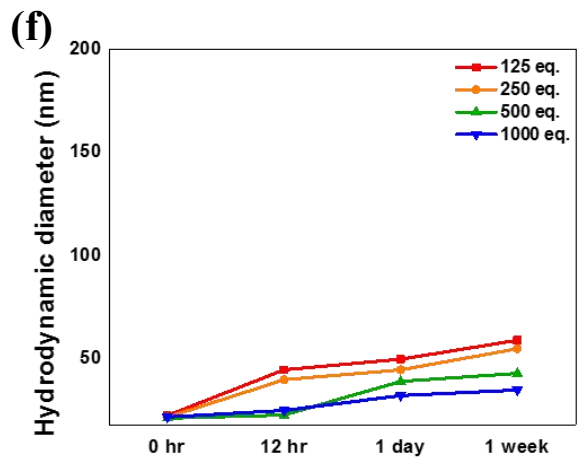
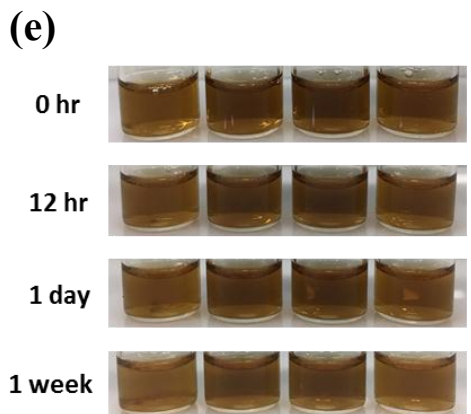
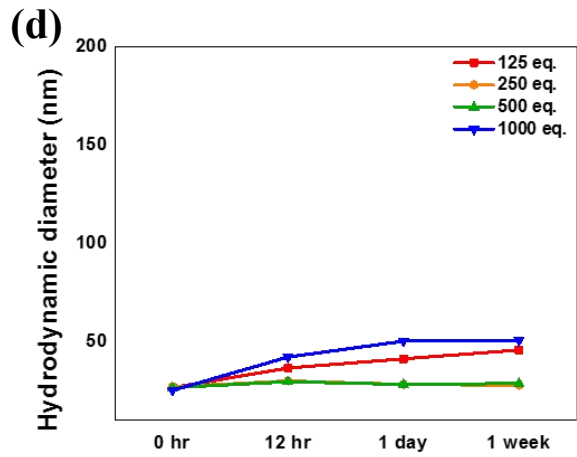
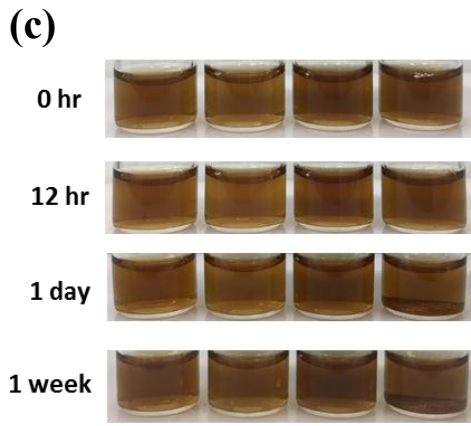
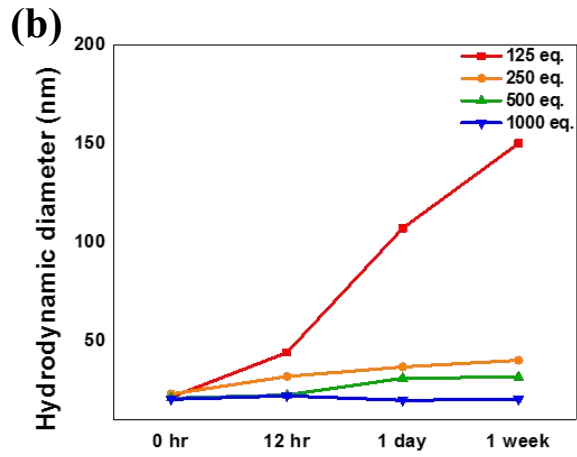
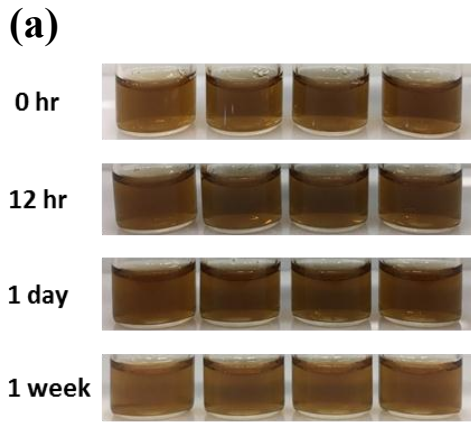
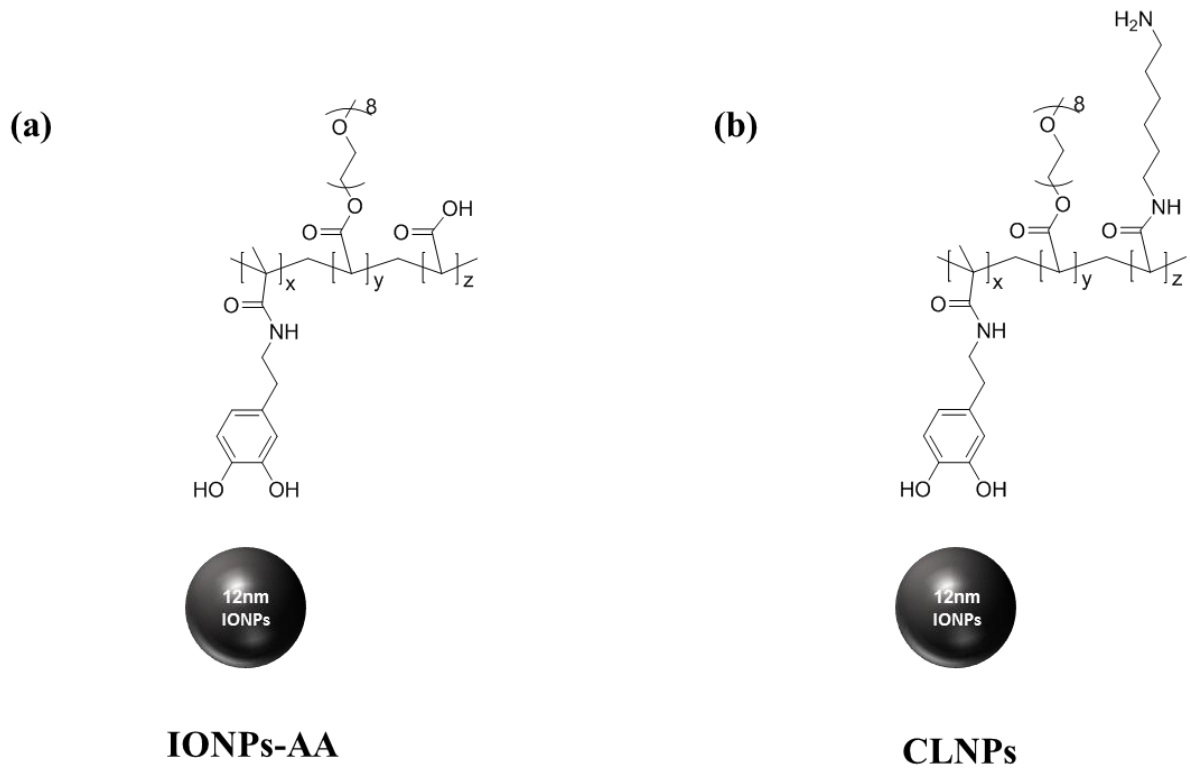


Figure 11. Camera image of stability test in pH 3 of CLNPs with (a) EDM (c) HDM and (e) BHTM. Their HD sizes in time consuming stability were measured by DLS (b) EDM (d) HDM and (f) BHTM used CLNPs.

2.3.3 Confirmation of cross linked IONPs (CLNPs)

To ensure the cross-linking reaction was applied to IONPs appropriately, confirmation was made using CLNPs with 250 eq. of HDM by X-ray photon spectroscopy (XPS), TEM analysis. First, TEM analysis was attempted for the visualization of the presence of the CLNPs (figure 12). To visualize organic polymers with TEM, the negative staining with 2 wt% of phosphotungstic acid method is mainly used³¹. Prior to visualization experiments, CLNPs polymer was expected to maintain particle size. For TEM analysis, etched IONPs and CLNPs with 4 M of HCl solution were prepared, then extracted polymer by chloroform solvent. The negative stained of the extracted polymer was confirmed by TEM. As a result, the cross-linked polymer was found to maintain larger size than uncross-linked polymer (figure 12). This suggests that some of the ligands bound to the surface of CLNPs may be retained. Also, by DLS measurement, the size of IONPs polymer was ~2 nm but the CLNPs polymer was maintained larger size (figure 12e). The reason for this phenomenon is that when the polymer ligand has a certain concentration or more, it forms a spherical shape of micelle, so that the polymer without cross linking could be maintained as spherical when it was confirmed by TEM.

XPS spectra was used to make quantitative and reliable confirmation of CLNPs. IONPs and CLNPs were prepared for comparison of cross-linking reaction (scheme 4). N1s and C1s peak of each NPs were analyzed for comparison of difference between the presence of cross-linking (figure 13). First, comparing the N1s peak of NPs (figure 13c,d), before cross-linking, the amide bond of DMA and the amine bond of coating reagent (CR) amino ethoxy ethanol (AEE) were confirmed by XPS peak 399.5 eV, 398.2 eV⁶⁰. However, 401.8 eV. peak was detected in CLNPs XPS spectra which represents the primary amine peak from cross-linked HDM. As the primary amine peak is formed, the CR amine peak is relatively decreased and the amide bond peak of diamine and carboxyl is increased. As a result, it can be shown that amide bond is formed due to EDC coupling. At the same time C1s XPS peak was analyzed (figure 13a,b). for the comparison with each NPs, the C1s XPS spectra was performed by normalization based on PEG C-O ether group. When diamine was used for cross-linking reaction, the content of C-C/C-H bond is increased from 108.7% to 185.6%. This result indicates that the HDM was involved in cross-linking of IONPs by EDC coupling with carboxylic acid of the IONPs surface.



Scheme 4. Scheme of the (a) IONPs-AA and (b) CLNPs with 125 eq. of HDM to compare N1s and C1s energy binding peak analyzed by XPS spectra.

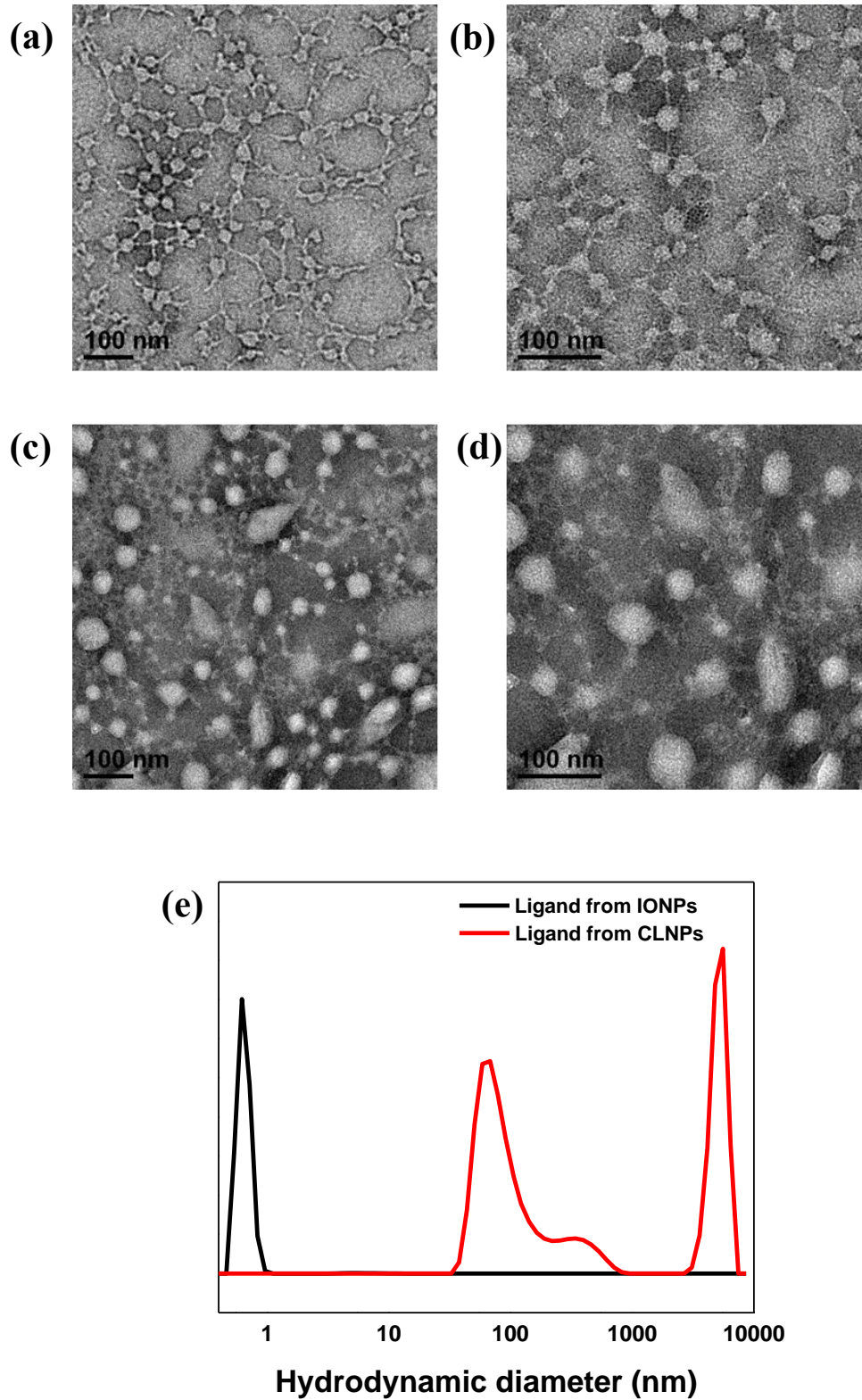


Figure 12. Visualization of polymer with 1 wt% of phosphotungstic acid, IONPs polymer by TEM magnification (a) 50 k and (b) 100 k, CLNPs polymer in (c) 50 k and (d) 100 k. (e) DLS data of these extracted polymer.

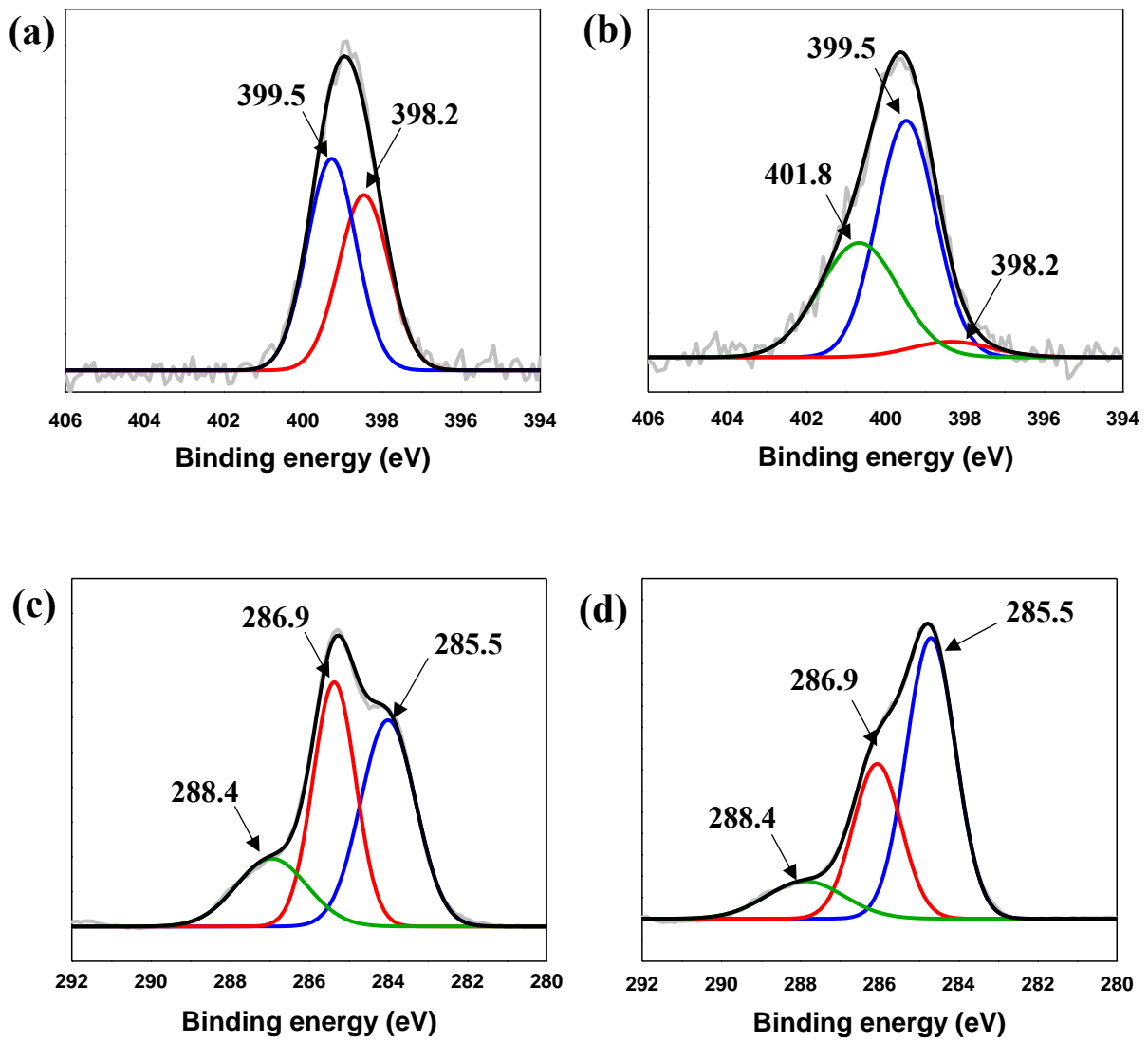


Figure 13. XPS spectra of C1s peak fitting of (a) IONPs and (b) CLNPs with HDM. N1s peak fitting of (c) IONPs and (d) CLNPs

2.3.4 Various stability test of CLNPs

The greatest advantage of the cross-linking is that the stability of the IONPs is maximized. Research on colloidal stability of bio-application nanoparticles has been done for many years^{13, 56, 61}. Although there have been many studies of enhancing stability, there have not been many reports on the validation of colloidal stability. In this research, various verification tools for the colloidal stability were proposed and the stability of CLNPs was confirmed.

Applications of IONPs in vitro and in vivo always include high dilutions of NPs dispersions, also, stability under high salt concentrations and over a range of pHs must be retained²². Therefore, IONPs required sufficient stability to endure long circulation time in bio media. For approve the enhanced stability of CLNPs, three compositions of NPs were dispersed in broad range of pH (pH 3-11) solution and measured changes of sizes with DLS for a week (figure 14). The cross-linking condition used in this experiment was the most stable 250 eq. of HDM condition among the three diamines identified in the previous experiment. In the case of IONPs composed of DMA30% PEG₄₈₀70% ligand (IONPs-PEG) (figure 14a), IONPs-PEG became unstable at pH 3 buffer solution after 1 day, as shown in camera image, aggregates occurred after one week. The size of IONPs-PEG measured with DLS was significantly increased. In the case of IONPs composed of DMA30% PEG₄₈₀40% Acrylic acid30% ligand (IONPs-AA) (figure 14b), also became unstable in pH 3 buffer solution. However, there was a difference from the IONPs-PEG condition. This result indicates the negative charge of acrylic acid assisted dispersion in buffer solution with charge repulsion. Unlike the other IONPs, CLNPs stayed stable in all of pH range for a week because of cross-linking reaction ensured stability of IONPs (figure 14c). stability of IONPs dispersions to excess electrolytes (NaCl) exhibited a similar trend (figure 15). In the case of IONPs-PEG became unstable after 1 day in high concentration of NaCl (3 M), DLS measurement result shows that the size of IONPs-PEG was dramatically increased after 1 day in all concentrations of NaCl conditions (figure 15a). As similar with the previous results, IONPs-AA was more stable than IONP-PEG in NaCl solution (figure 15b). This is also the result of charge repulsion due to the acrylic acid negative part. Still, became unstable in high concentration of NaCl solution (3 M). To overcome these unstable conditions, CLNPs retained their size in NaCl at each concentration, which proved the stability of CLNPs (figure 15c). In addition, unlike previous studies, the size variation of IONPs under various conditions was studied in detail and stability of IONPs was compared.

Since the stability was improved, an experiment was conducted to confirm that it was stable in further reaction. For bio application of NPs, the general conjugation method called 'click' chemistry is used for conjugation of bio molecules to NPs because of its rapid, specific, and robust conjugation reaction. However, the 'click' chemistry reaction takes place under harsh conditions such as of 1 mM of copper sulfate and 5 mM of ascorbic acid solution. So, it is a challenge to be

stable in the harsh condition for conjugation of bio molecules. These difficulties can be complemented by CLNPs (figure 16). As shown in the figure, IONPs and CLNPs were compared the stability in the 'click' chemistry reaction condition. In the case of IONPs, which were uncross-linked, all degradation occurred and precipitated were formed (figure 16a). Unlike this, CLNPs were stable and change of size was not observed after 24 hr (figure 16b, d). These results suggest that bio-application without any aggregation is possible even with application of CLNPs to the azide-alkyne conjugation method. The stability at high temperature was confirmed by treated IONPs in 95°C of oil bath (figure 16e). Only the size of IONPs-PEG was increased after treated several minutes. On the other hand, IONPs-AA stayed stable as CLNPs, the reason for this result is that the partial acid part of acrylic acid has a role on the surface to some extent. Finally, the stability in purification step was compared. Also, the similar result was exhibited that as the number of viva spin increases, only IONPs-PEG became unstable (figure 16f). These various tools were used to confirm the stability of the particles and the possibility of further reaction of CLNPs.

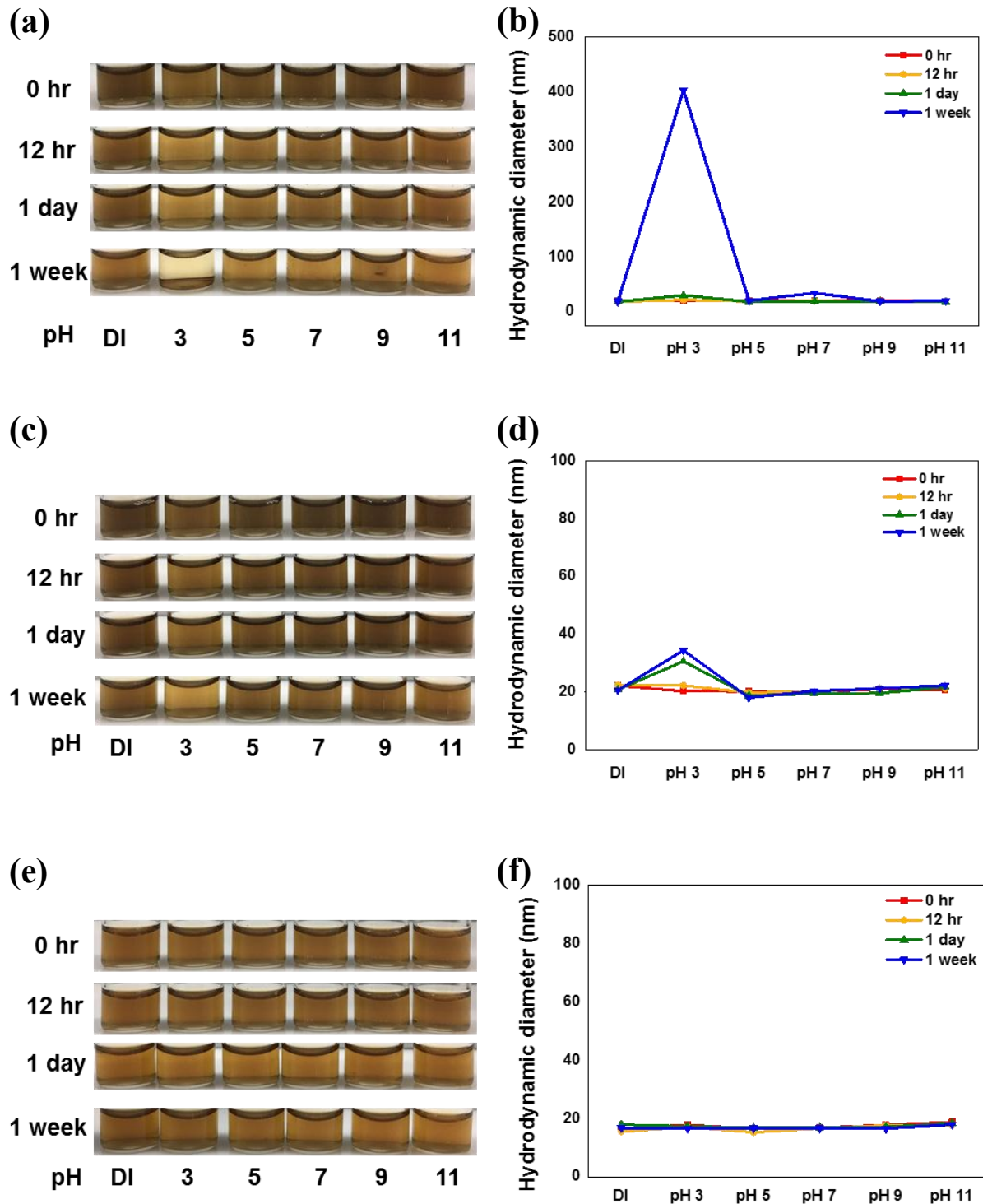
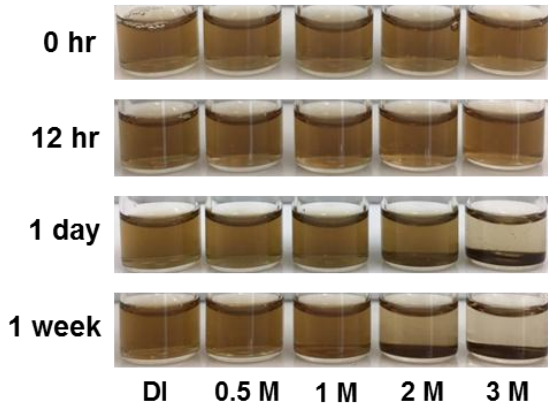
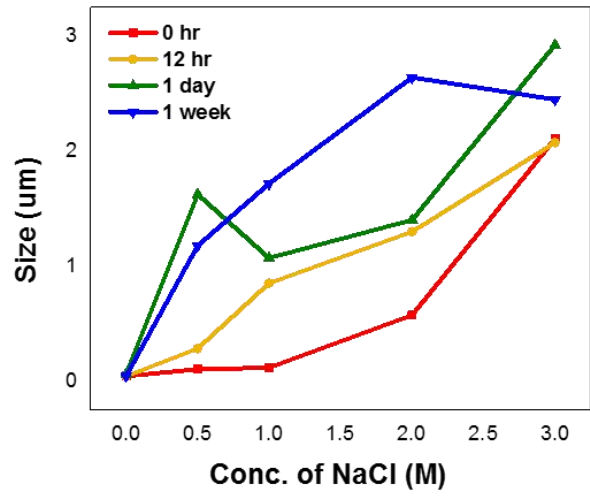


Figure 14. Camera image of stability of (a) IONPs-PEG (c) IONPs-AA and (e) CLNPs in wide range of pHs. Graph of hydrodynamic diameter about time consuming results in various pHs (b) IONPs-PEG (d) IONPs-AA and (f) CLNPs.

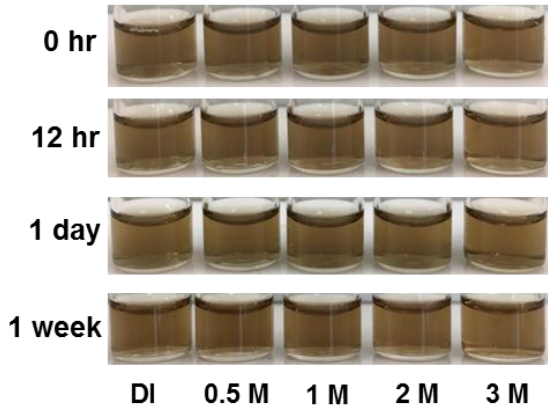
(a)



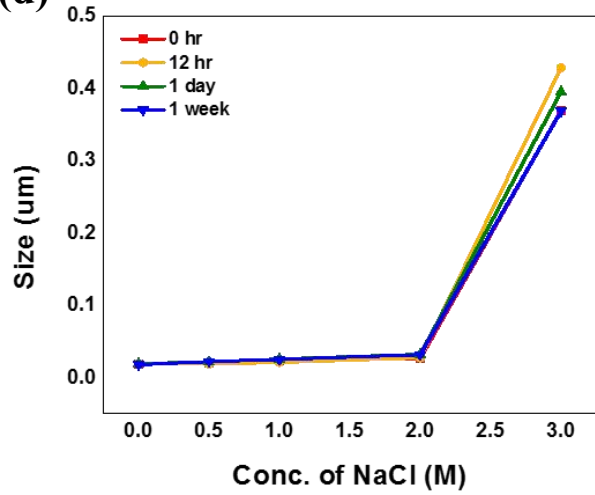
(b)



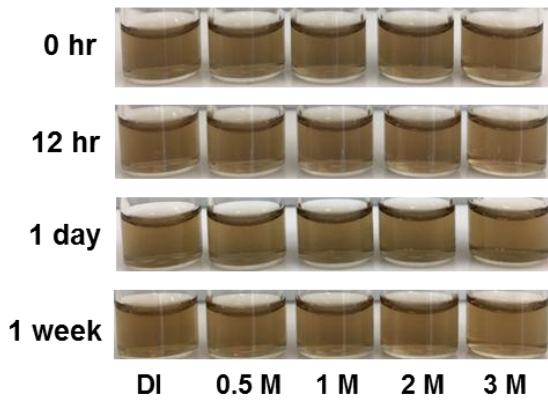
(c)



(d)



(e)



(f)

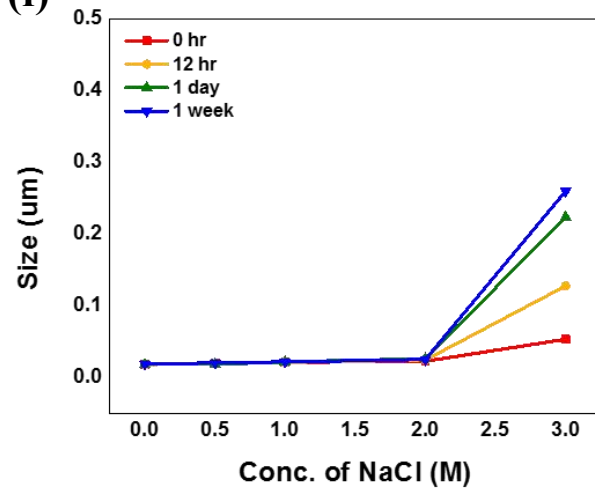


Figure 15. Camera image of stability of (a) IONPs-PEG (c) IONPs-AA and (e) CLNPs in various concentrations of NaCl solutions. Graph of hydrodynamic diameter about time consuming results in NaCl solutions of (b) IONPs-PEG (d) IONPs-AA and (f) CLNPs.

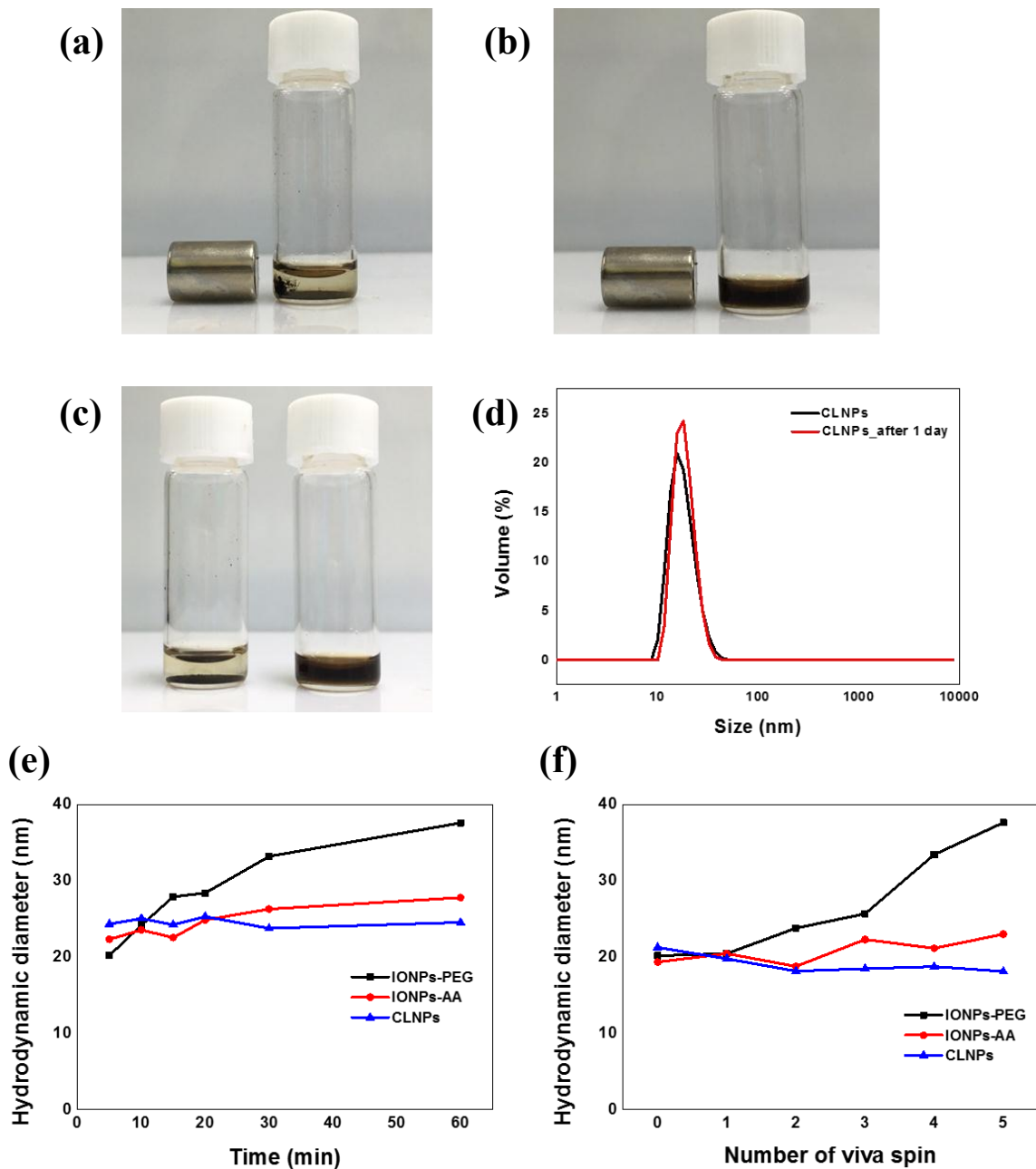


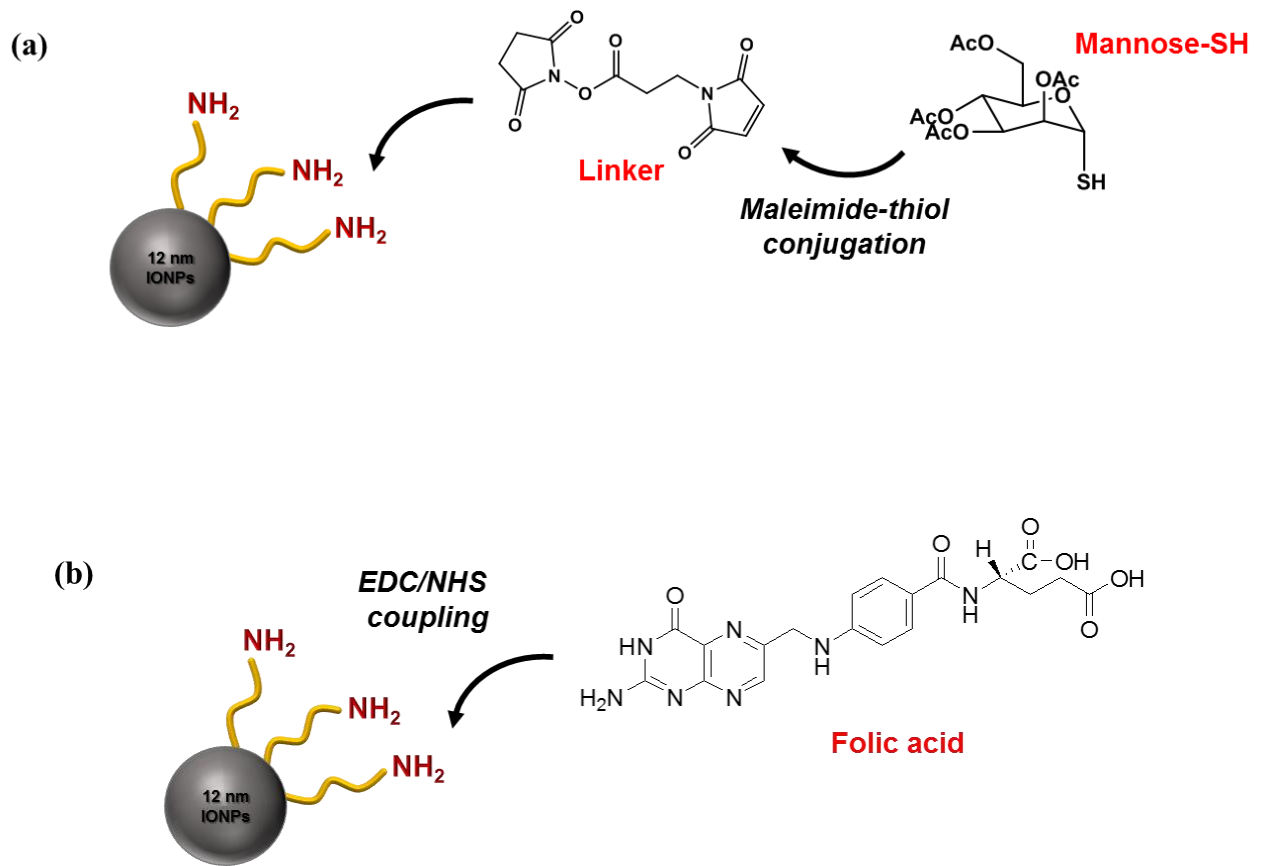
Figure 16. Stability test in click chemistry conditions with (a) IONPs-PEG (b) CLNPs (c) 24 h later in click chemistry condition IONPs-PEG (left) and CLNPs (right) and (d) measured with DLS. (e) stability test of thermal effect in 95 °C condition. (f) hydrodynamic diameters were measured to observe the effect of purification with viva spin.

2.3.5 Multifunctional conjugation of CLNPs

Functional groups of NPs are essential for bio application such as cancer cell targeting and drug delivery⁶²⁻⁶³. CLNPs are multifunctional nanoparticles with stability and functionalization characteristics at the same time. In previous experiments, as the amine functionalization of CLNPs were confirmed by RITC conjugation (figure 9). With this known accessible amine group of CLNPs, several bio molecules were conjugation experiments were performed (scheme 5).

First, one of the monosaccharide types, mannose (Man) was conjugated to CLNPs for confirmation of amine functionalization. This glycoconjugates such as mannose, glucose, and galactose are attractive substance for targeting receptor-mediated interaction. It has advantages of easy synthesis process and targeting ability with specific lectins⁶⁴. To conjugated thiolated mannose (Man-SH) to amine functionalized CLNPs, the linker was essential for maleimide-thiol specific conjugation (scheme 5a). After CLNPs-Man conjugation, dialysis at pH 11 buffer process was necessary for deprotection of acetyl protected group of Man, solvent exchange, and purification of excess molecules. After all processes and re-dispersed in 1xPBS buffer, the size of CLNPs-Man was compact without any aggregates (figure 17). The conjugation of CLNPs-Man was analyzed by High resolution magic angle spinning (HR-MAS) (figure 18). Signal from 3.5 - 3.6 ppm indicates specific peak of mannose. To separate signal for more detailed analysis, the signal 3.65 ppm indicates the organic ligand of CLNPs. Further analysis was performed with Fourier transform infrared (FT-IR) (figure 19). The O-H bond from carboxyl group wavelength from 920 - 990 cm^{-1} decreases in CLNPs-Man signal, also the appearance of amide peak 1650-1720 cm^{-1} indicates cross-linked part. In addition, 1248 cm^{-1} C-N peak was identified as maleimide group and sulfide bond from Man-SH maleimide conjugates was identified in wavelength 604 cm^{-1} .

Based on the above conjugation result, another bio molecule called folic acid was conjugated to CLNPs (scheme 5b). Folic acid has strong binding affinity with folate receptor which expressed in human malignant cell membranes such as cancers of ovary, kidney, lung, breast, and liver. When folic acid conjugated NPs bind to the folate receptor, cell targeting occurred by the endocytosis^{45, 65}. With this properties and advantages of inexpensive and stable in bio media, it's application of NPs are widely researched for decades. After conjugation of folic acid to CLNPs process, the size of CLNPs-FA seemed to maintain stable HD size ~ 24 nm without any aggregation (Figure 20a). UV-Vis analysis was used for confirmation of CLNPs-FA (figure 20b). Since the folic acid has specific absorbance in wavelength 285 and 360 nm, this specific peak was observed in CLNPs-FA UV-Vis graph. In the case of CLNPs, the dopamine peak at 280 nm was observed but nothing at 360 nm. With this result, CLNPs-FA were formed successfully and indicates that CLNPs are highly stable in any other reactions, also amine groups of CLNPs are accessible for the bio conjugation.



Scheme 5. Scheme of multifunctional CLNPs conjugated with (a) mannose and (b) folic acid

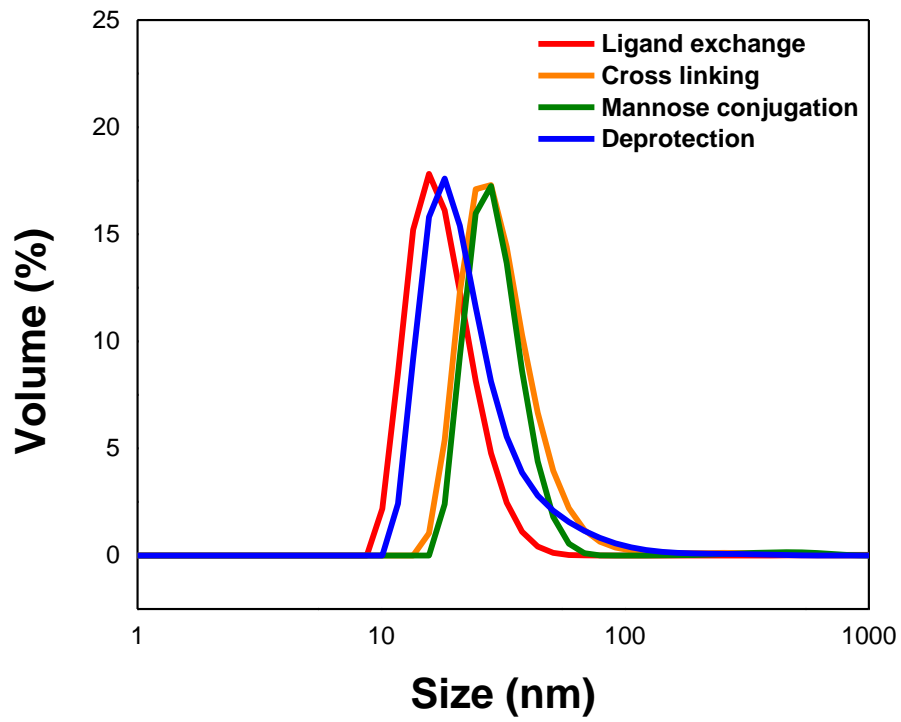


Figure 17. DLS data of CLNPs-Man indicates no aggregates while further reactions.

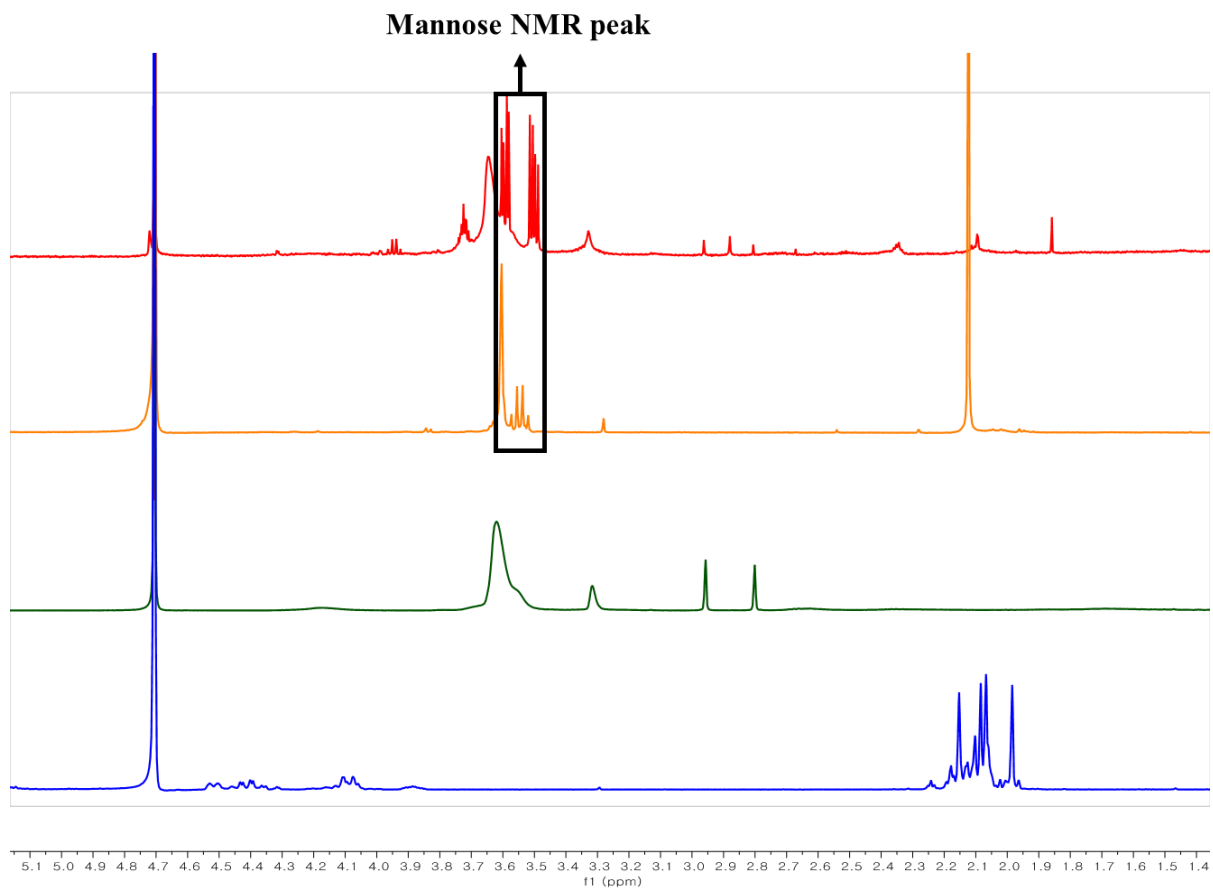


Figure 18. HR-MAS data of CLNP-Man (red), Man-SH (yellow), Polymer ligand (green), and Acetyl protected Man-SH (blue) in D₂O solvent.

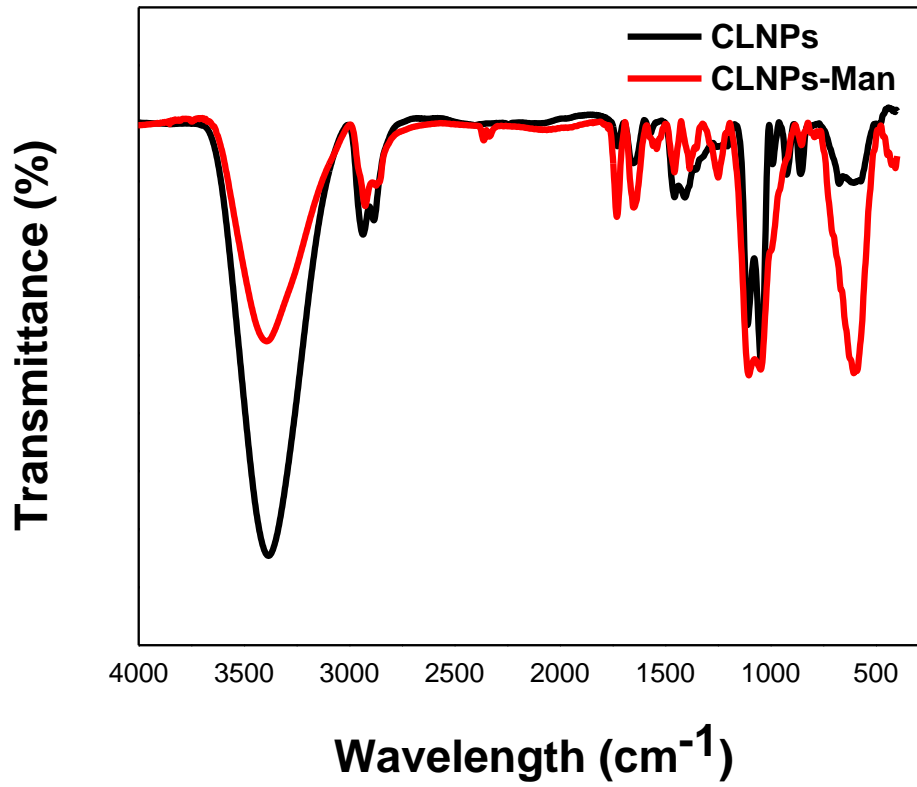


Figure 19. FT-IR data of CLNPs (black) and CLNPs-Man (red) to confirm the mannose conjugated CLNPs.

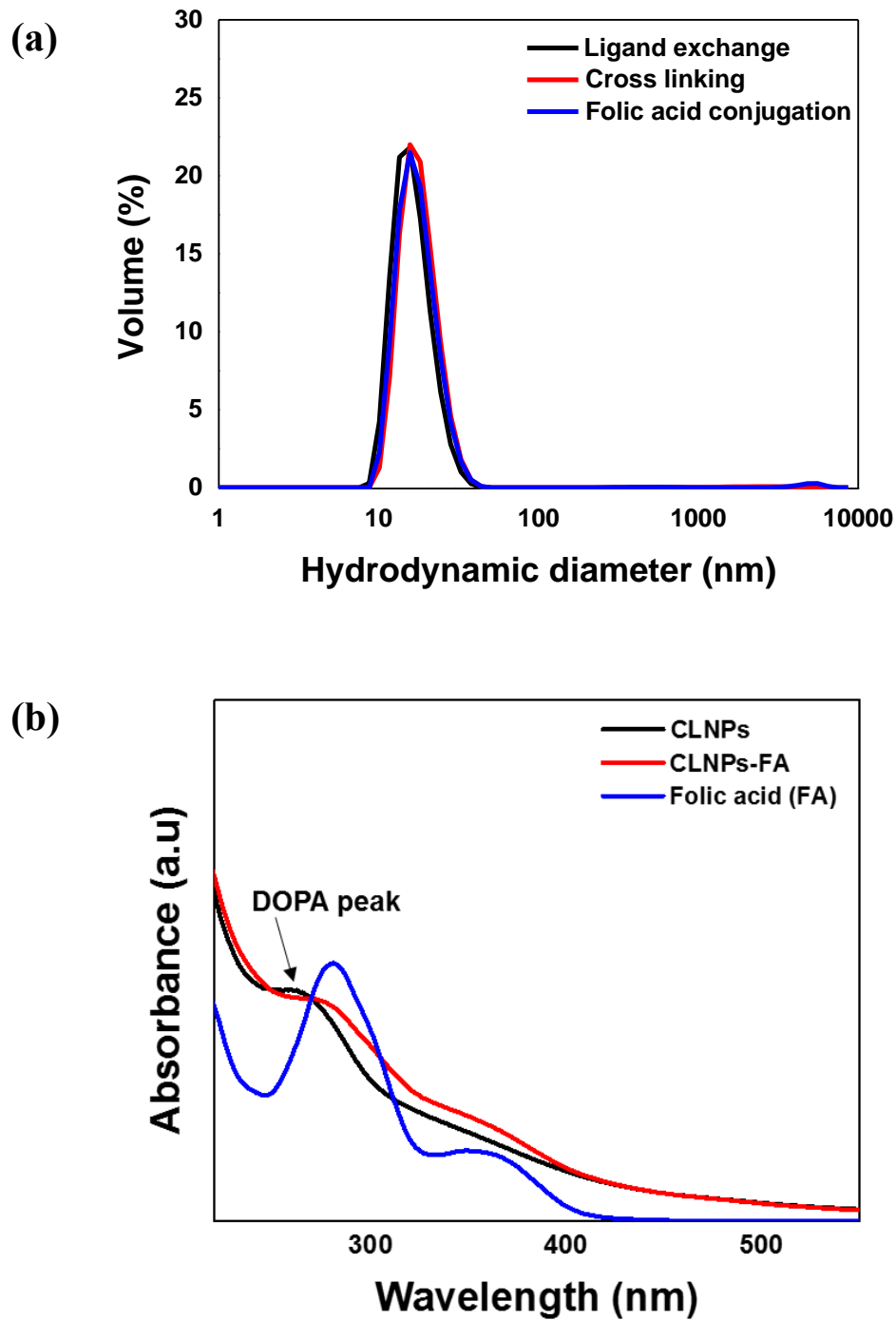
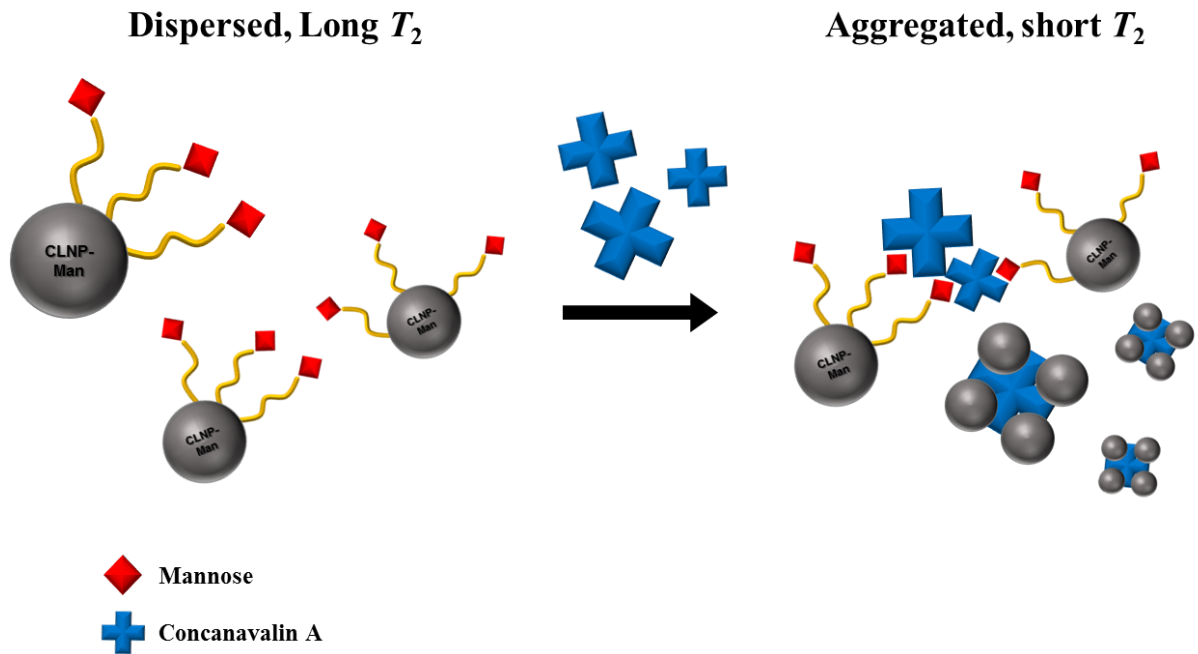


Figure 20. (a) DLS data of after folic acid conjugated to CLNPs (b) UV-Vis absorbance analysis to confirm folic acid conjugation.

2.3.6 specific targeting test by MR relaxivity

Although CLNPs-Man were synthesized, it is important to that the carbohydrates immobilized on CLNPs retain their biological recognition specificity. This was proved using addition of mannose specific recognized lectin Concanavalin A (Con A) into CLNPs-Man. This process was measured by magnetic resonance relaxivity through Minispec analysis. It is well known that since the magnetic moment of a nanoparticle is proportional to its volume, the R_2 relaxivity increases with IONPs size⁷. Based on this background, when IONPs become agglomerate like cluster form, the local magnetic field gradients increases at the same time, so surrounding water molecules spin dephasing occurred efficiently⁶⁶⁻⁶⁷. Because of these characteristics, T_2 relaxation time is reduced and the contrast effect is increased and it will appear darker imaging on MRI (scheme 6).

First, upon incubation of a Con A lectin with IONPs and CLNPs-Man, confirmed that mannose conjugated to CLNPs was retained its biological recognition. Significant decrease of T_2 relaxation value was observed in CLNPs-Man (Figure 21a). This is because that Con A has four binding sites for mannose conjugation, so when CLNPs-Man interacted with Con A, CLNPs became agglomerated which effect decrease of T_2 relaxation time. Unlike CLNPs-Man, CLNPs without mannose have no change in T_2 relaxation after addition of Con A (Figure 21a). To further validate the specificity, glucose specific recognition lectin wheat germ agglutinin (WGA) lectin was used instead of Con A (figure 21b). As shown in the graph, there was no difference in T_2 relaxation time when the WGA was added to CLNPs-Man while Con A was effective. Through these results, mannose which immobilized in CLNPs retain their biological recognition specificity, indeed, application of CLNPs in vitro and in vivo targeting potencies were confirmed.



Scheme 6. Scheme of CLNPs-Man incubated with Con A resulted in the formation of aggregates, leading to shorter T_2 relaxation time and consequently a darkened MRI image.

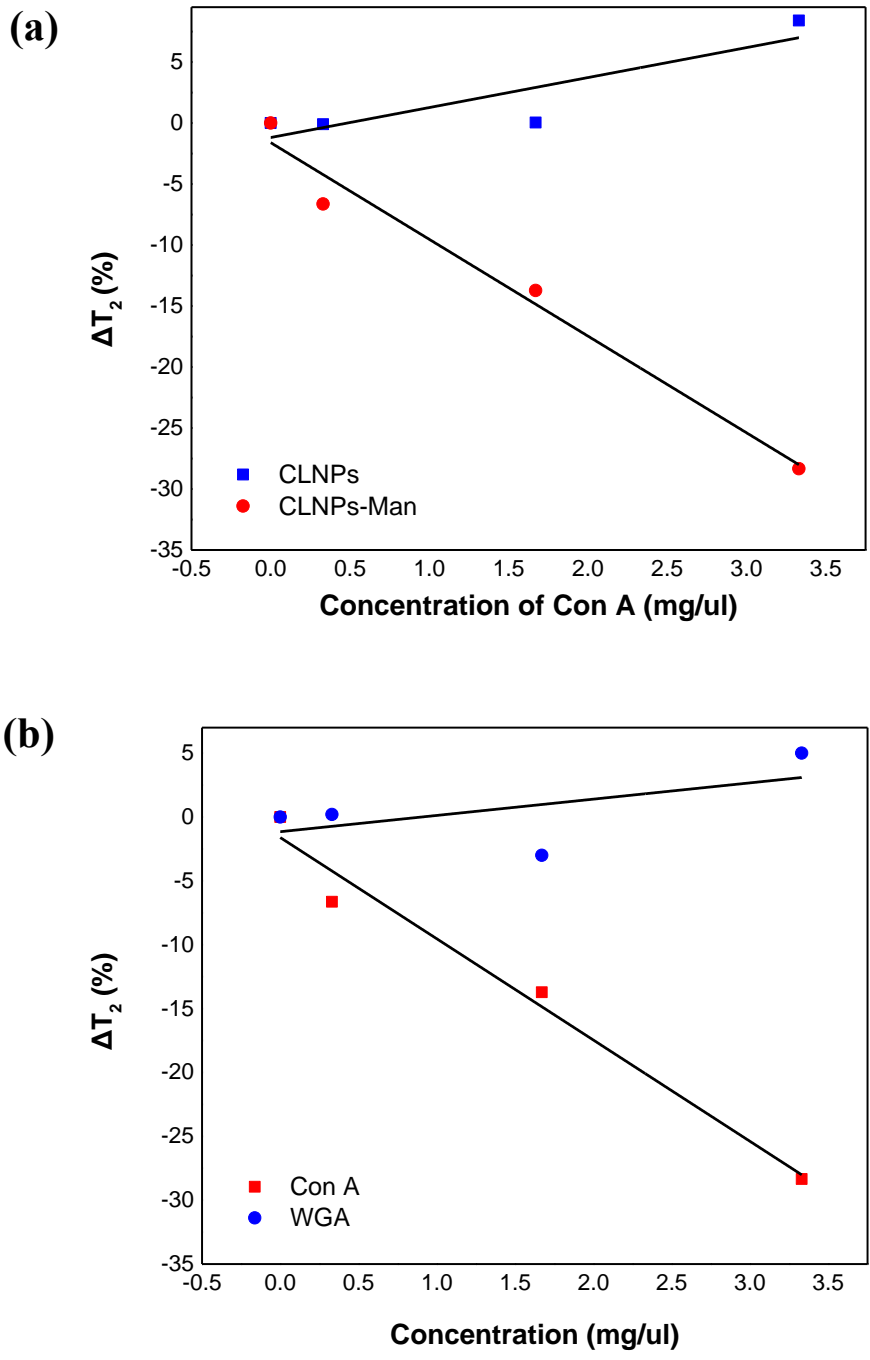
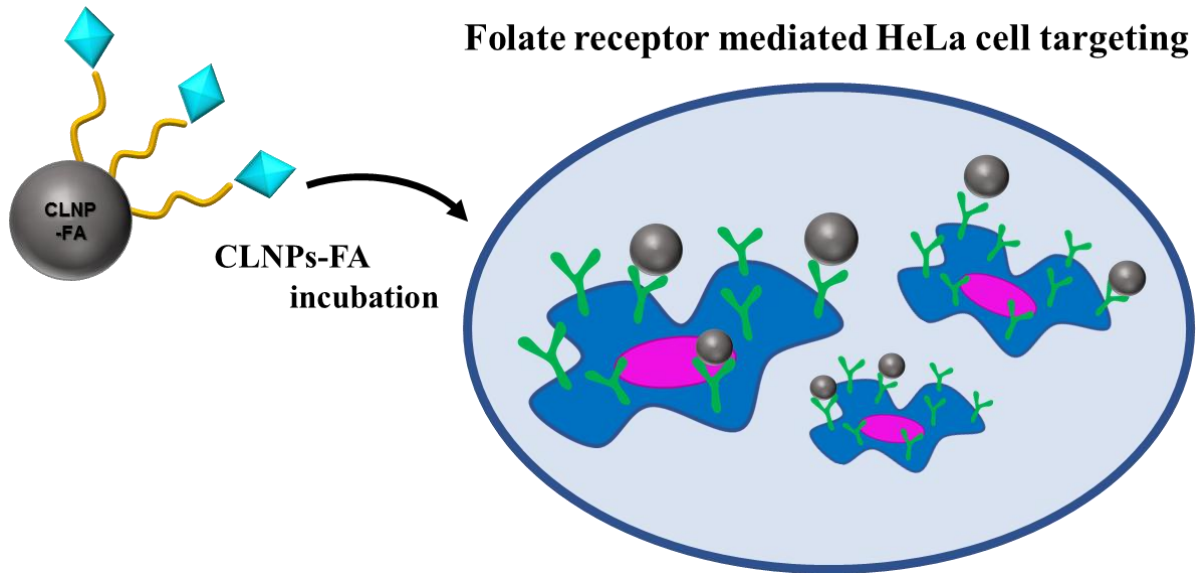


Figure 21. Graph of MR T₂ relaxivity (a) with addition of Con A to CLNP (blue) and CLNP-Man (red). (b) changes of T₂ relaxivity of CLNPs-Man using different lectins Con A (red) and WGA (blue).

2.3.7 In vitro test with folic acid conjugated CLNPs

As shown in the above experiment, since it was confirmed that the bio molecules retain their characteristics even after conjugation, folic acid was conjugated to CLNPs for in vivo targeting test. Folic acid mediated in vitro targeting experiment was performed in HeLa cell. Characterized CLNPs-FA (figure 20b) and normal CLNPs were incubated to HeLa cell for 6 hours. In this case, the concentrations of NPs were set to 200 and 500 μ M. To verify cellular uptake of IONPs, Prussian blue staining method is mainly used because Prussian blue can be reacted with magnetite core, then the intense blue color can be performed⁶⁸. After Prussian blue staining, the HeLa cell was observed with inverted fluorescence microscopy (figure 22). There was no blue staining in HeLa cells treated with normal CLNPs, while CLNPs-FA treated HeLa cells were stained in blue as the result of highly specific targeting and uptake by folate receptor. These results indicate folic acid presented in CLNPs drastically recognizes folate receptor and capable in vitro system.



Scheme 7. Scheme of folate receptor mediated HeLa cell targeting with CLNPs-FA.

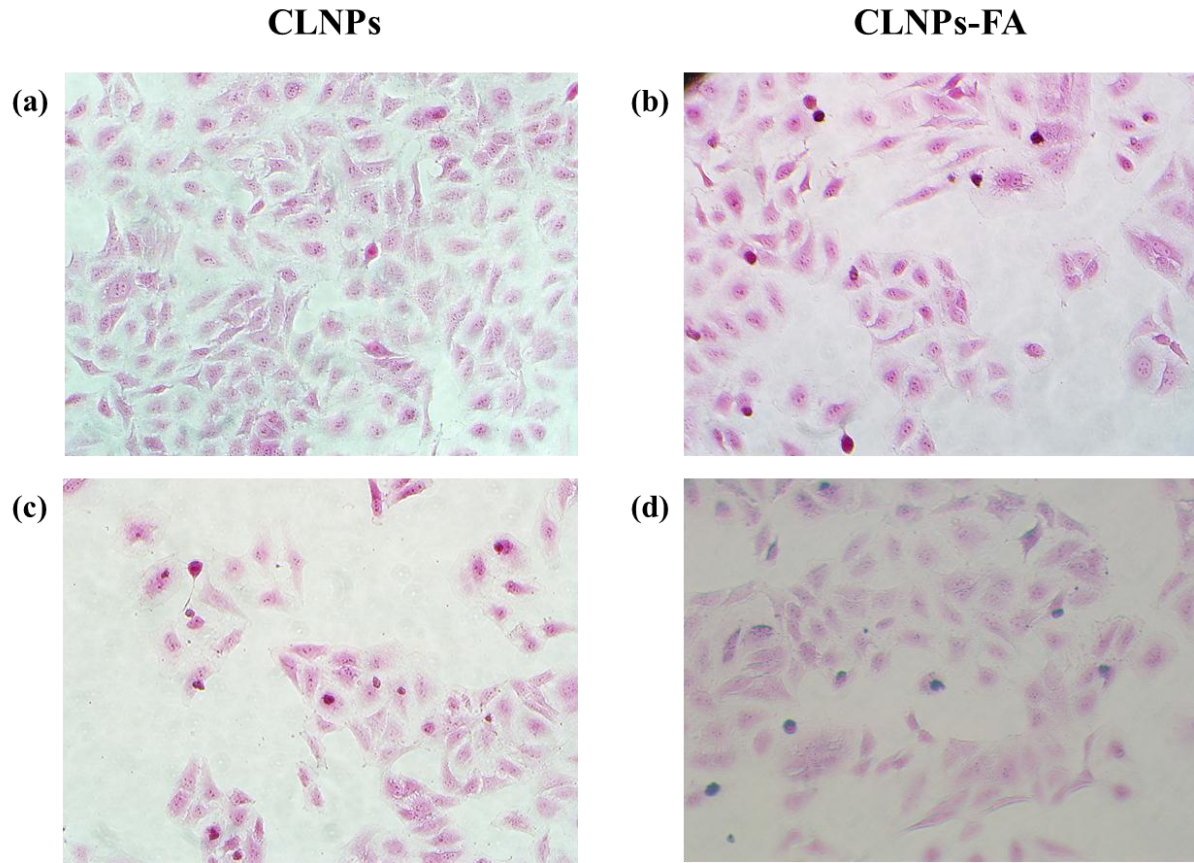


Figure 22. Microscopy image of Prussian blue stained HeLa cell treated with (a) 200 uM and (c) 500 uM of CLNPs. (b) 200 uM and (d) 500 uM of CLNPs-FA.

2.4 Conclusion

In this research, highly stable and amine functionalized compact IONPs were developed by cross-linking reaction with EDC coupling. Firstly, ligand of the composition suitable for uniform IONPs was synthesized. The ligand was composed of catechol dopamine methacrylamide (DMA) which has strong binding affinity with iron ion, poly(ethylene glycol) (PEG) as hydrophilic part, and carboxyl acid as functional group by RAFT polymerization system. Through this optimization experiment, the ligand composited DMA 30% PEG480 40% AA 30% was used for ligand exchanged with coating reagent AEE to impart compact thin coating and hydrophilic function of IONPs. Furthermore, effect of cross linking by EDC coupling using various lengths of diamines was performed, and compared the stability difference and the degree of amine functionalization in IONPs.

Also, in this research, proposed a means to clearly compare the stability of the CLNPs by confirming the stability of the CLNPs through various tools such as XPS spectra, TEM visualization, click chemistry condition, time consuming size change in wide range of pHs and NaCl. Moreover, the fact CLNPs were highly stable in click chemistry condition, indicates possibility of azide-alkyne bio molecules conjugation system can be applied to CLNPs process for rapid and rigid conjugation. As high stability was established, CLNPs have amine functional group at the same time. To confirm these amine groups are available for bio conjugation, mannose and folic acid were conjugated. After all of procedures, there was no aggregation of CLNPs conjugates, and characterized with HR-MAS, FT-IR, and UV-Vis. MR imaging and cancer cell targeting test showed that the conjugated bio molecules retained their properties after conjugation to CLNPs. Through these sufficient proofs of CLNPs bio applications, NPs based on this nano-platform system have potential to being applied to real bio applications such as drug delivery, MR imaging, and hyperthermia therapy.

By developing the platform that can enhance the stability of the NPs and facilitate the functionalization by the simple cross-linking method, it is expected that can facilitate the bio application of various NPs other than IONPs.

III. References

1. Lee, J.-H.; Kim, J.-w.; Cheon, J., Magnetic Nanoparticles for Multi-Imaging and Drug Delivery. *Molecules and Cells* **2013**, *35* (4), 274-284.
2. Reddy, L. H.; Arias, J. L.; Nicolas, J.; Couvreur, P., Magnetic Nanoparticles: Design and Characterization, Toxicity and Biocompatibility, Pharmaceutical and Biomedical Applications. *Chemical Reviews* **2012**, *112* (11), 5818-5878.
3. Park, J.; An, K.; Hwang, Y.; Park, J. G.; Noh, H. J.; Kim, J. Y.; Park, J. H.; Hwang, N. M.; Hyeon, T., Ultra-large-scale syntheses of monodisperse nanocrystals. *Nat Mater* **2004**, *3* (12), 891-5.
4. Ling, D.; Lee, N.; Hyeon, T., Chemical synthesis and assembly of uniformly sized iron oxide nanoparticles for medical applications. *Acc Chem Res* **2015**, *48* (5), 1276-85.
5. Roberts, W. G.; Palade, G. E., Neovasculature Induced by Vascular Endothelial Growth Factor Is Fenestrated. *Cancer Research* **1997**, *57* (4), 765.
6. Kim, B. H.; Lee, N.; Kim, H.; An, K.; Park, Y. I.; Choi, Y.; Shin, K.; Lee, Y.; Kwon, S. G.; Na, H. B.; Park, J. G.; Ahn, T. Y.; Kim, Y. W.; Moon, W. K.; Choi, S. H.; Hyeon, T., Large-scale synthesis of uniform and extremely small-sized iron oxide nanoparticles for high-resolution T1 magnetic resonance imaging contrast agents. *J Am Chem Soc* **2011**, *133* (32), 12624-31.
7. Lee, N.; Hyeon, T., Designed synthesis of uniformly sized iron oxide nanoparticles for efficient magnetic resonance imaging contrast agents. *Chem Soc Rev* **2012**, *41* (7), 2575-89.
8. Oz, Y.; Arslan, M.; Gevrek, T. N.; Sanyal, R.; Sanyal, A., Modular Fabrication of Polymer Brush Coated Magnetic Nanoparticles: Engineering the Interface for Targeted Cellular Imaging. *ACS Applied Materials & Interfaces* **2016**, *8* (30), 19813-19826.
9. <35_INVEST RADIOL 2011, 46(7), 441-449.pdf>
10. Zhu, X.; Lin, H.; Wang, L.; Tang, X.; Ma, L.; Chen, Z.; Gao, J., Activatable T1 Relaxivity Recovery Nanoconjugates for Kinetic and Sensitive Analysis of Matrix Metalloprotease 2. *ACS Applied Materials & Interfaces* **2017**, *9* (26), 21688-21696.
11. Chan, N.; Laprise-Pelletier, M.; Chevallier, P.; Bianchi, A.; Fortin, M. A.; Oh, J. K., Multidentate block-copolymer-stabilized ultrasmall superparamagnetic iron oxide nanoparticles with enhanced colloidal stability for magnetic resonance imaging. *Biomacromolecules* **2014**, *15* (6), 2146-56.
12. Na, H. B.; Palui, G.; Rosenberg, J. T.; Ji, X.; Grant, S. C.; Mattoussi, H., Multidentate Catechol-Based Polyethylene Glycol Oligomers Provide Enhanced Stability and Biocompatibility to Iron Oxide Nanoparticles. *ACS Nano* **2012**, *6* (1), 389-399.
13. Li, P.; Chevallier, P.; Ramrup, P.; Biswas, D.; Vuckovich, D.; Fortin, M.-A.; Oh, J. K., Mussel-Inspired Multidentate Block Copolymer to Stabilize Ultrasmall Superparamagnetic Fe₃O₄ for Magnetic Resonance Imaging Contrast Enhancement and Excellent Colloidal Stability. *Chemistry of Materials* **2015**, *27* (20), 7100-7109.

14. Johnson, N. J. J.; He, S.; Nguyen Huu, V. A.; Almutairi, A., Compact Micellization: A Strategy for Ultrahigh T1 Magnetic Resonance Contrast with Gadolinium-Based Nanocrystals. *ACS Nano* **2016**, *10* (9), 8299-8307.
15. Lu, C.-W.; Hung, Y.; Hsiao, J.-K.; Yao, M.; Chung, T.-H.; Lin, Y.-S.; Wu, S.-H.; Hsu, S.-C.; Liu, H.-M.; Mou, C.-Y.; Yang, C.-S.; Huang, D.-M.; Chen, Y.-C., Bifunctional Magnetic Silica Nanoparticles for Highly Efficient Human Stem Cell Labeling. *Nano Letters* **2007**, *7* (1), 149-154.
16. Susumu, K.; Uyeda, H. T.; Medintz, I. L.; Pons, T.; Delehanty, J. B.; Mattoussi, H., Enhancing the Stability and Biological Functionalities of Quantum Dots via Compact Multifunctional Ligands. *Journal of the American Chemical Society* **2007**, *129* (45), 13987-13996.
17. Jun, Y.-w.; Huh, Y.-M.; Choi, J.-s.; Lee, J.-H.; Song, H.-T.; KimKim; Yoon, S.; Kim, K.-S.; Shin, J.-S.; Suh, J.-S.; Cheon, J., Nanoscale Size Effect of Magnetic Nanocrystals and Their Utilization for Cancer Diagnosis via Magnetic Resonance Imaging. *Journal of the American Chemical Society* **2005**, *127* (16), 5732-5733.
18. Na, H. B.; Lee, I. S.; Seo, H.; Park, Y. I.; Lee, J. H.; Kim, S. W.; Hyeon, T., Versatile PEG-derivatized phosphine oxide ligands for water-dispersible metal oxide nanocrystals. *Chem Commun (Camb)* **2007**, (48), 5167-9.
19. Wei, H.; Insin, N.; Lee, J.; Han, H.-S.; Cordero, J. M.; Liu, W.; Bawendi, M. G., Compact Zwitterion-Coated Iron Oxide Nanoparticles for Biological Applications. *Nano Letters* **2012**, *12* (1), 22-25.
20. Park, Y. I.; Kim, E.; Huang, C.-H.; Park, K. S.; Castro, C. M.; Lee, H.; Weissleder, R., Facile Coating Strategy to Functionalize Inorganic Nanoparticles for Biosensing. *Bioconjugate Chemistry* **2017**, *28* (1), 33-37.
21. Laurent, S.; Forge, D.; Port, M.; Roch, A.; Robic, C.; Vander Elst, L.; Muller, R. N., Magnetic Iron Oxide Nanoparticles: Synthesis, Stabilization, Vectorization, Physicochemical Characterizations, and Biological Applications. *Chemical Reviews* **2008**, *108* (6), 2064-2110.
22. Amstad, E.; Textor, M.; Reimhult, E., Stabilization and functionalization of iron oxide nanoparticles for biomedical applications. *Nanoscale* **2011**, *3* (7), 2819-43.
23. Shubayev, V. I.; Pisanic, T. R.; Jin, S., Magnetic nanoparticles for theragnostics. *Advanced drug delivery reviews* **2009**, *61* (6), 467-477.
24. Mosqueira, V. C. F.; Legrand, P.; Morgat, J.-L.; Vert, M.; Mysiakine, E.; Gref, R.; Devissaguet, J.-P.; Barratt, G., Biodistribution of Long-Circulating PEG-Grafted Nanocapsules in Mice: Effects of PEG Chain Length and Density. *Pharmaceutical Research* **2001**, *18* (10), 1411-1419.
25. Wang, Y.-X. J.; Hussain, S. M.; Krestin, G. P., Superparamagnetic iron oxide contrast agents: physicochemical characteristics and applications in MR imaging. *European Radiology* **2001**, *11* (11), 2319-2331.
26. Moore, A.; Marecos, E.; Bogdanov, A.; Weissleder, R., Tumoral Distribution of Long-circulating

- Dextran-coated Iron Oxide Nanoparticles in a Rodent Model. *Radiology* **2000**, *214* (2), 568-574.
27. Högemann, D.; Josephson, L.; Weissleder, R.; Basilion, J. P., Improvement of MRI Probes To Allow Efficient Detection of Gene Expression. *Bioconjugate Chemistry* **2000**, *11* (6), 941-946.
 28. Lewin, M.; Carlesso, N.; Tung, C.-H.; Tang, X.-W.; Cory, D.; Scadden, D. T.; Weissleder, R., Tat peptide-derivatized magnetic nanoparticles allow in vivo tracking and recovery of progenitor cells. *Nature Biotechnology* **2000**, *18*, 410.
 29. Park, J.; Yu, M. K.; Jeong, Y. Y.; Kim, J. W.; Lee, K.; Phan, V. N.; Jon, S., Antibiofouling amphiphilic polymer-coated superparamagnetic iron oxide nanoparticles: synthesis, characterization, and use in cancer imaging in vivo. *Journal of Materials Chemistry* **2009**, *19* (35), 6412.
 30. Lee, H.; Yu, M. K.; Park, S.; Moon, S.; Min, J. J.; Jeong, Y. Y.; Kang, H.-W.; Jon, S., Thermally Cross-Linked Superparamagnetic Iron Oxide Nanoparticles: Synthesis and Application as a Dual Imaging Probe for Cancer in Vivo. *Journal of the American Chemical Society* **2007**, *129* (42), 12739-12745.
 31. Yang, H. M.; Park, C. W.; Lim, S.; Park, S. I.; Chung, B. H.; Kim, J. D., Cross-linked magnetic nanoparticles from poly(ethylene glycol) and dodecyl grafted poly(succinimide) as magnetic resonance probes. *Chem Commun (Camb)* **2011**, *47* (46), 12518-20.
 32. Chung, H. J.; Lee, H.; Bae, K. H.; Lee, Y.; Park, J.; Cho, S.-W.; Hwang, J. Y.; Park, H.; Langer, R.; Anderson, D.; Park, T. G., Facile Synthetic Route for Surface-Functionalized Magnetic Nanoparticles: Cell Labeling and Magnetic Resonance Imaging Studies. *ACS Nano* **2011**, *5* (6), 4329-4336.
 33. Pösel, E.; Kloust, H.; Tromsdorf, U.; Janschel, M.; Hahn, C.; Maßlo, C.; Weller, H., Relaxivity Optimization of a PEGylated Iron-Oxide-Based Negative Magnetic Resonance Contrast Agent for T2-Weighted Spin-Echo Imaging. *ACS Nano* **2012**, *6* (2), 1619-1624.
 34. Wang, L.; Huang, J.; Chen, H.; Wu, H.; Xu, Y.; Li, Y.; Yi, H.; Wang, Y. A.; Yang, L.; Mao, H., Exerting Enhanced Permeability and Retention Effect Driven Delivery by Ultrafine Iron Oxide Nanoparticles with T1-T2 Switchable Magnetic Resonance Imaging Contrast. *ACS Nano* **2017**, *11* (5), 4582-4592.
 35. Iatridi, Z.; Vamvakidis, K.; Tsougos, I.; Vassiou, K.; Dendrinou-Samara, C.; Bokias, G., Multifunctional Polymeric Platform of Magnetic Ferrite Colloidal Superparticles for Luminescence, Imaging, and Hyperthermia Applications. *ACS Applied Materials & Interfaces* **2016**, *8* (51), 35059-35070.
 36. Ulbrich, K.; Holá, K.; Šubr, V.; Bakandritsos, A.; Tuček, J.; Zbořil, R., Targeted Drug Delivery with Polymers and Magnetic Nanoparticles: Covalent and Noncovalent Approaches, Release Control, and Clinical Studies. *Chemical Reviews* **2016**, *116* (9), 5338-5431.
 37. Lee, J.-H.; Lee, K.; Moon, S. H.; Lee, Y.; Park, T. G.; Cheon, J., All-in-One Target-Cell-Specific

- Magnetic Nanoparticles for Simultaneous Molecular Imaging and siRNA Delivery. *Angewandte Chemie International Edition* **2009**, *48* (23), 4174-4179.
38. Espinosa, A.; Di Corato, R.; Kolosnjaj-Tabi, J.; Flaud, P.; Pellegrino, T.; Wilhelm, C., Duality of Iron Oxide Nanoparticles in Cancer Therapy: Amplification of Heating Efficiency by Magnetic Hyperthermia and Photothermal Bimodal Treatment. *ACS Nano* **2016**, *10* (2), 2436-2446.
 39. Thorat, N. D.; Bohara, R. A.; Noor, M. R.; Dhamecha, D.; Soulimane, T.; Tofail, S. A. M., Effective Cancer Theranostics with Polymer Encapsulated Superparamagnetic Nanoparticles: Combined Effects of Magnetic Hyperthermia and Controlled Drug Release. *ACS Biomaterials Science & Engineering* **2017**, *3* (7), 1332-1340.
 40. Li, L.; Jiang, W.; Luo, K.; Song, H.; Lan, F.; Wu, Y.; Gu, Z., Superparamagnetic Iron Oxide Nanoparticles as MRI contrast agents for Non-invasive Stem Cell Labeling and Tracking. *Theranostics* **2013**, *3* (8), 595-615.
 41. Na, H. B.; Song, I. C.; Hyeon, T., Inorganic Nanoparticles for MRI Contrast Agents. *Advanced Materials* **2009**, *21* (21), 2133-2148.
 42. Wei, H.; Bruns, O. T.; Kaul, M. G.; Hansen, E. C.; Barch, M.; Wisniowska, A.; Chen, O.; Chen, Y.; Li, N.; Okada, S.; Cordero, J. M.; Heine, M.; Farrar, C. T.; Montana, D. M.; Adam, G.; Ittrich, H.; Jasanoff, A.; Nielsen, P.; Bawendi, M. G., Exceedingly small iron oxide nanoparticles as positive MRI contrast agents. *Proc Natl Acad Sci U S A* **2017**, *114* (9), 2325-2330.
 43. Qi, H.; Liu, C.; Long, L.; Ren, Y.; Zhang, S.; Chang, X.; Qian, X.; Jia, H.; Zhao, J.; Sun, J.; Hou, X.; Yuan, X.; Kang, C., Blood Exosomes Endowed with Magnetic and Targeting Properties for Cancer Therapy. *ACS Nano* **2016**, *10* (3), 3323-33.
 44. Sonvico, F.; Mornet, S.; Vasseur, S.; Dubernet, C.; Jaillard, D.; Degrouard, J.; Hoebeke, J.; Duguet, E.; Colombo, P.; Couvreur, P., Folate-Conjugated Iron Oxide Nanoparticles for Solid Tumor Targeting as Potential Specific Magnetic Hyperthermia Mediators: Synthesis, Physicochemical Characterization, and in Vitro Experiments. *Bioconjugate Chemistry* **2005**, *16* (5), 1181-1188.
 45. Shen, J. M.; Guan, X. M.; Liu, X. Y.; Lan, J. F.; Cheng, T.; Zhang, H. X., Luminescent/magnetic hybrid nanoparticles with folate-conjugated peptide composites for tumor-targeted drug delivery. *Bioconjug Chem* **2012**, *23* (5), 1010-21.
 46. Zhang, W.; Yu, Z. L.; Wu, M.; Ren, J. G.; Xia, H. F.; Sa, G. L.; Zhu, J. Y.; Pang, D. W.; Zhao, Y. F.; Chen, G., Magnetic and Folate Functionalization Enables Rapid Isolation and Enhanced Tumor-Targeting of Cell-Derived Microvesicles. *ACS Nano* **2017**, *11* (1), 277-290.
 47. Wong, C.; Stylianopoulos, T.; Cui, J.; Martin, J.; Chauhan, V. P.; Jiang, W.; Popović, Z.; Jain, R. K.; Bawendi, M. G.; Fukumura, D., Multistage nanoparticle delivery system for deep penetration into tumor tissue. *Proceedings of the National Academy of Sciences* **2011**, *108* (6), 2426-2431.
 48. Kievit, F. M.; Zhang, M., Surface Engineering of Iron Oxide Nanoparticles for Targeted Cancer Therapy. *Accounts of Chemical Research* **2011**, *44* (10), 853-862.

49. Li, M.; Kim, H. S.; Tian, L.; Yu, M. K.; Jon, S.; Moon, W. K., Comparison of Two Ultrasmall Superparamagnetic Iron Oxides on Cytotoxicity and MR Imaging of Tumors. *Theranostics* **2012**, *2* (1), 76-85.
50. Yang, Y.; Li, Y.; Lin, Q.; Bao, C.; Zhu, L., In Situ Phototriggered Disulfide-Cross-Link Nanoparticles for Drug Delivery. *ACS Macro Letters* **2016**, *5* (3), 301-305.
51. Gupta, A. K.; Gupta, M., Synthesis and surface engineering of iron oxide nanoparticles for biomedical applications. *Biomaterials* **2005**, *26* (18), 3995-4021.
52. Guo, J.; Filpponen, I.; Johansson, L. S.; Mohammadi, P.; Latikka, M.; Linder, M. B.; Ras, R. H.; Rojas, O. J., Complexes of Magnetic Nanoparticles with Cellulose Nanocrystals as Regenerable, Highly Efficient, and Selective Platform for Protein Separation. *Biomacromolecules* **2017**, *18* (3), 898-905.
53. Park, J. W.; Ku, S. H.; Moon, H. H.; Lee, M.; Choi, D.; Yang, J.; Huh, Y. M.; Jeong, J. H.; Park, T. G.; Mok, H.; Kim, S. H., Cross-linked iron oxide nanoparticles for therapeutic engineering and in vivo monitoring of mesenchymal stem cells in cerebral ischemia model. *Macromol Biosci* **2014**, *14* (3), 380-9.
54. Quinto, C. A.; Mohindra, P.; Tong, S.; Bao, G., Multifunctional superparamagnetic iron oxide nanoparticles for combined chemotherapy and hyperthermia cancer treatment. *Nanoscale* **2015**, *7* (29), 12728-36.
55. Lee, C. S.; Chang, H. H.; Bae, P. K.; Jung, J.; Chung, B. H., Bifunctional Nanoparticles Constructed Using One-Pot Encapsulation of a Fluorescent Polymer and Magnetic (Fe₃O₄) Nanoparticles in a Silica Shell. *Macromolecular Bioscience* **2013**, *13* (3), 321-331.
56. Palui, G.; Aldeek, F.; Wang, W.; Mattoussi, H., Strategies for interfacing inorganic nanocrystals with biological systems based on polymer-coating. *Chem Soc Rev* **2015**, *44* (1), 193-227.
57. Yoo, D.; Jeong, H.; Noh, S. H.; Lee, J. H.; Cheon, J., Magnetically triggered dual functional nanoparticles for resistance-free apoptotic hyperthermia. *Angew Chem Int Ed Engl* **2013**, *52* (49), 13047-51.
58. Yim, Y. S.; Choi, J. S.; Kim, G. T.; Kim, C. H.; Shin, T. H.; Kim, D. G.; Cheon, J., A facile approach for the delivery of inorganic nanoparticles into the brain by passing through the blood-brain barrier (BBB). *Chem Commun (Camb)* **2012**, *48* (1), 61-3.
59. Lee, H.; Lee, B. P.; Messersmith, P. B., A reversible wet/dry adhesive inspired by mussels and geckos. *Nature* **2007**, *448*, 338.
60. Tischer, T.; Claus, T. K.; Bruns, M.; Trouillet, V.; Linkert, K.; Rodriguez-Emmenegger, C.; Goldmann, A. S.; Perrier, S.; Börner, H. G.; Barner-Kowollik, C., Spatially Controlled Photochemical Peptide and Polymer Conjugation on Biosurfaces. *Biomacromolecules* **2013**, *14* (12), 4340-4350.
61. Mondini, S.; Drago, C.; Ferretti, A. M.; Puglisi, A.; Ponti, A., Colloidal stability of iron oxide

- nanocrystals coated with a PEG-based tetra-catechol surfactant. *Nanotechnology* **2013**, *24* (10), 105702.
62. Neoh, K. G.; Kang, E. T., Functionalization of inorganic nanoparticles with polymers for stealth biomedical applications. *Polymer Chemistry* **2011**, *2* (4), 747-759.
 63. Steichen, S. D.; Caldorera-Moore, M.; Peppas, N. A., A review of current nanoparticle and targeting moieties for the delivery of cancer therapeutics. *European Journal of Pharmaceutical Sciences* **2013**, *48* (3), 416-427.
 64. El-Boubbou, K.; Zhu, D. C.; Vasileiou, C.; Borhan, B.; Prospero, D.; Li, W.; Huang, X., Magnetic Glyco-Nanoparticles: A Tool To Detect, Differentiate, and Unlock the Glyco-Codes of Cancer via Magnetic Resonance Imaging. *Journal of the American Chemical Society* **2010**, *132* (12), 4490-4499.
 65. Yang, S.-J.; Lin, F.-H.; Tsai, K.-C.; Wei, M.-F.; Tsai, H.-M.; Wong, J.-M.; Shieh, M.-J., Folic Acid-Conjugated Chitosan Nanoparticles Enhanced Protoporphyrin IX Accumulation in Colorectal Cancer Cells. *Bioconjugate Chemistry* **2010**, *21* (4), 679-689.
 66. Norek, M.; A. Pereira, G.; Geraldos, C.; Denkova, A.; Zhou, W.; Peters, J., *NMR Transversal Relaxivity of Suspensions of Lanthanide Oxide Nanoparticles*. 2007; Vol. 111.
 67. Thorek, D. L.; Chen, A. K.; Czupryna, J.; Tsourkas, A., Superparamagnetic iron oxide nanoparticle probes for molecular imaging. *Ann Biomed Eng* **2006**, *34* (1), 23-38.
 68. Lee, H.; Lee, E.; Kim, D. K.; Jang, N. K.; Jeong, Y. Y.; Jon, S., Antibiofouling Polymer-Coated Superparamagnetic Iron Oxide Nanoparticles as Potential Magnetic Resonance Contrast Agents for in Vivo Cancer Imaging. *Journal of the American Chemical Society* **2006**, *128* (22), 7383-7389.